HHS Public Access

Author manuscript

Biomater Sci. Author manuscript; available in PMC 2021 March 31.

Published in final edited form as:

Biomater Sci. 2020 March 31; 8(7): 1783–1801. doi:10.1039/c9bm01787a.

Microfluidics for ZnO Micro-/Nanomaterials Development: Rational Design, Controllable Synthesis, and On-Chip Bioapplications

Nanjing Hao[a,c], **Michael Zhang**[b,c], **John X.J. Zhang**[a,*]

[a]Thayer School of Engineering, Dartmouth College, 14 Engineering Drive, Hanover, New Hampshire 03755, United States.

[b]The Lawrenceville School, 2500 Main St, Lawrenceville, New Jersey 08648, United States

Abstract

Zinc oxide (ZnO) materials hold great promise in diverse applications due to their attractive physicochemical features. Recent years, especially in the last decade, have witnessed a considerable progress toward rational design and bioapplications of multiscale ZnO materials through microfluidic techniques. Design of microfluidic device that allows for precise control over reaction conditions could not only yield ZnO particles with fast production rate and high quality, but also permit downstream applications with desirable and superior performance. This review summarizes microfluidic approaches for the synthesis and applications of ZnO micro-/nanomaterials. In particular, we discuss recent achievement of using microfluidic reactors in the controllable synthesis of ZnO structures (wire, rod, sphere, flower, sheet, flake, spindle, and ellipsoid), and highlight the unprecedented opportunities for applying them in biosensing, biological separation, and molecular catalysis applications through microfluidic chips. Finally, major challenges and potential opportunities are explored to guide future studies in this area.

Graphical Abstract

* john.zhang@dartmouth.edu.

[c]These two authors contributed equally.

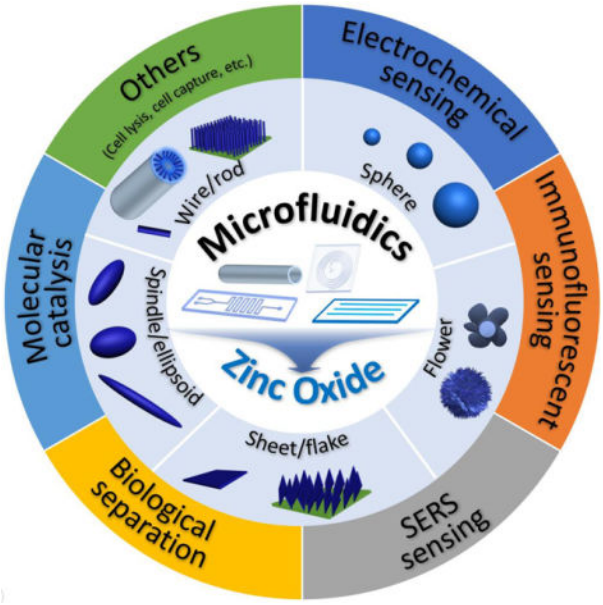

Keywords

Microfluidics; Microreactor; Zinc Oxide; On-Chip; Microchip

1. Introduction

Zinc oxide (ZnO) micro-/nanomaterials have attracted great attention from material scientists and engineers due to their remarkable properties and wide potential applications in optoelectronics,[1] energy,[2] biomedical engineering,[3] catalysis and environment.[4] To date, a large variety of ZnO materials with distinct physicochemical properties have been developed using methods such as hydrothermal, sol-gel, supercritical fluid, spray pyrolysis, biosynthesis, and physical/chemical vapor deposition.[5,6] Taking advantage of well-established batch processes and rich kinds of reactant systems, ZnO structures with controllable sizes (from few nanometers to tens of micrometers) and shapes (such as wire, rod, sphere, ellipsoid, flower, cube, sheet, and plate) are already available. However, facing the relatively low reproducibility and poor control over conventional batch reaction processes, it is still in great demand to develop delicate and elaborate methods for meeting the practical needs of diverse fields.

The emergence of microfluidics brings a variety of new and attractive features that conventional batch systems can hardly achieve, such as real-time spatio-temporal control, high flexibility and integration capability, and low samples consumption.[7–10] From the upstream materials synthesis point of view, microfluidics-based microreactors could offer many unique advantages over conventional flask-based batch reactors. For examples, rapid reaction kinetics and dedicated control of reaction parameters enable fast screening and optimization of material properties; greatly reduced reactor dimensions and large surface-to-volume ratio of microchannels allow enhanced mass/heat transfer, leading to minimal batch-to-batch difference and high yields; and working at elevated temperatures and pressures

while confining potentially active starting reactants gives great chances to create new materials.[11–20] Therefore, microreactors have been widely employed for controllable synthesis of polymers,[21–27] gold,[28,29] quantum dots,[30,31] magnetic materials,[32] and silica materials.[33] Similarly, from the downstream application point of view, microfluidics-based microchips could provide many superior benefits over conventional batch approaches, such as high sensitivity and specificity, rapid response time, simple sample pretreatment, and low sample consumption. These features endow microchips with promising potential applications in sensing,[34,35] catalysis,[28,36] nanomedicine,[25] drug delivery,[37–40] tissue engineering,[24] and many other biomedical fields.[20,41–44]

This review first presents an overview of recent progress on the synthesis and applications of ZnO micro-/nanomaterials using microfluidics. We start by summarizing the established continuous and discrete microreactor systems for the rational design and controllable synthesis of ZnO structures, followed by highlighting the unprecedented opportunities of microchips in myriad applications of biosensing, biological separation, and molecular catalysis, and finally providing in-depth discussions of current challenges and opportunities for guiding future research.

2. Microfluidics fundamentals

Since emerged in the early 1980s, microfluidics technologies have become promising tools for a variety of applications.[7] Due to scaling down in dimensions, the fluid behavior is primarily dominated by viscosity rather than inertia, and high surface-to-volume ratio enables rapid mass and heat transfer in microfluidic devices. These features provide great opportunities in the field of synthetic and analytical chemistry, biology, and engineering sciences.

For on-chip materials synthesis and applications of ZnO, Reynolds number (*Re*) that gives a measure of the ratio of inertial forces to viscous forces is usually used to predict the flow conditions. The Reynolds number is expressed as $Re = \rho UL/\mu$, where ρ is the fluid density, U is the flow velocity, L is the characteristic length of microchannel, and μ is the fluid dynamic viscosity. Generally, flow in microfluidic reactors is always laminar due to the microscale dimensions. Although the laminar flow inside microfluidic devices allows for more controllable reactions, it causes obvious diffusion-limited mixing of reactants. To overcome this inherent issue, active or passive mixing modules are proposed in different forms.[14,20] Optimizing the design of microfluidic reactors toward enhanced mixing performance is guided by Péclet number (*Pe*) that represents the ratio of advection and diffusion caused by heat transfer. The Péclet number can be expressed as $Pe = UL/D$, where U is an average flow velocity, L is a representative length scale, and D is the diffusion coefficient. Since the typical values of U, L, and D in microchannels are ~1 m/s, 10^{-6}-10^{-4} m, and 10^{-10}-10^{-11} m^2/s, respectively, the Pe of microfluidic devices is thus relatively large enough to neglect the diffusion-limited mixing.[33] To improve the mixing performance of reactants for ZnO production, one common strategy is to increase the length of microchannels (such as winding or serpentine form). Given the homogeneous reaction environment from microfluidics, the production efficiency and working performance of resultant materials are generally higher than those from conventional batch reactors.

Therefore, microfluidics provides an excellent platform for rational design, controllable synthesis, and on-chip applications of functional ZnO materials.

The development of microfluidic devices followed the continuous growing demand for the synthesis and application of micro-/nanoparticles. The rapid growth of microfabrication techniques has led to the revolution of microfluidic reactors for ZnO materials synthesis as well as microfluidic chips for on-chip applications. The simplest design started with tubular straight microreactors made of glass capillary and stainless steel, which had the obvious advantages of low cost and easy scaling up. However, they could not meet the needs for complicated reactions, which thus stimulated the progress of polydimethylsiloxane (PDMS)-based microreactors fabricated by means of lithography techniques.[45] The combination of tubular and PDMS microreactors has also been utilized in some cases for meeting the synthesis and on-chip application requirements. However, there is still much room in microfluidic synthesis and application of ZnO micro-/nanomaterials.

3. Microfluidic synthesis of ZnO materials

Compared to conventional batch reactors (Figure 1A), microreactors could execute precise spatial-temporal control over experimental parameters such as microchannel dimensions, temperature, pressure, and flow rate, which enable the continuous synthesis of high quality ZnO micro-/nanoparticles with well-defined physicochemical properties. By virtue of their appealing features, microreactors have already successfully demonstrated the effectiveness of microfluidic approaches in the controllable production of ZnO materials with different sizes ranging from few nanometers to tens of micrometers and various shapes like wire, sphere, rod, flower, spindle, ellipsoid, and sheet (Table 1). Generally, microreactors for ZnO materials synthesis could be broadly grouped into two main categories: 1) continuous laminar flow microreactors that involve only one single phase aqueous fluids with two or multiple inlets for different reactants (Figure 1B); 2) discrete segmented flow microreactors that usually include one or more aqueous reactant fluids as inlets and one oil/gas phase for isolating aqueous flows (Figure 1C). Microreactors that introduce an immiscible oil flow as carrier liquid with several liquid flows of reactants are known as droplet flow microreactors (Figure 1C, left), while ones that include one gas phase flow to generate different segments of reactants are known as segmented flow microreactors (Figure 1C, right). In the following, we will systematically summarize the established microfluidic systems for the flow synthesis of ZnO micro-/nanoparticles.

3.1 Continuous laminar flow synthesis

Single phase continuous laminar flow synthesis approach is the most widely used for the controllable synthesis of ZnO materials inside specific microchannels where precursor reactants flow through and nucleation/growth processes take place. This type of microfluidic systems is generally simpler in structure and easier to operate, and thus demonstrating extensive control over reaction temperature and pressure, flow rates, resident time, and reactant concentration. In this section, we will discuss the capabilities of laminar flow microreactors in the synthesis of five main types of ZnO structure: wire/rod, sphere, flower, sheet/flake, and spindle/ellipsoid.

3.1.1 Wire/rod—Among all the available particle shapes of ZnO from microreactors, wire/rod has received the most intensive attention from researchers (Table 1). The flow synthesis of ZnO wire/rod is generally achieved by in-situ deposition onto underlying substrates inside microchannel in the form of ordered arrays (Figure 2). During the last decade, many approaches have been developed to synthesize ZnO nanowire/nanorod arrays with controllable structures. Chemical bath deposition (CBD) is one typical approach that allows ZnO materials to deposit on a heated glass/silicon substrate. However, conventional CBD always suffers from inefficient utilization of reactants and significant waste solvent generation.[60] The integration of microreactor with CBD has demonstrated to be a robust platform for the synthesis of high quality ZnO wire arrays. The plug-flow through microreactor exposes the substrate to bath composition that varies along the length of the reaction microchannel. Deposition at high flow rates results in more uniform nanowire arrays, whereas deposition at low flow rates leads to wider variation in nanowire length along the substrate (Figure 2A).[48,76] Specifically, along the flow direction, the length of nanowires decreased and the morphology changed from pyramidal tops to flat tops.[48,49] By modulating synthesis parameters such as the seeds preparation, residence time, and heating locations, ZnO nanowire arrays could be synthesized either on the entire substrate/patterned area,[53,57,78] or along the microheaters inside microchannel (Figure 2B).[53,65] However, it is noted that the fundamental issues for preparing vertical ZnO wire arrays are the rather slow deposition rate and the variation of reactant concentrations as a function of time.[68] To solve these, microreactor-assisted nanoparticle deposition system was developed to obtain highly uniform ZnO nanowire arrays with a growth rate as fast as 240 nm/min and an aspect ratio of nanowires up to 23 (Figure 2C). In addition to vertical growth, ZnO wire arrays can also grow horizontally by arranged micropost arrays (Figure 2D)[54] or by a set of high aspect ratio trenches (Figure 2E).[58] To densely pack ZnO nanowires, atomic layer deposition technique was demonstrated to be an effective tool to enable high coverage over the substrates (especially non-lateral or curved ones).[58] Considering only limited surface contact area that could be provided from both vertical growth and horizontal growth methods, researchers further successfully constructed three-dimensional nanowire arrays on the inner surface of confined glass capillary microchannels (Figure 2F).[50,67,73,80] These studies demonstrate the capability of continuous flow microreactors in the controllable synthesis of ZnO fiber/rod arrays with low cost, high efficiency, tunable structure, and flexible orientation, providing great potentials for practical applications in biosensing, biological separation, and molecular catalysis (as discussed in section 3).

3.1.2 Sphere—Since the feasibility of microfluidic flow synthesis of ZnO nanospheres was first demonstrated in 2004,[46] an increasing number of laminar flow synthesis approaches with distinct microreactor structures have been developed (Figure 3). Based on the supercritical coflowing microreactor, UV emitting ZnO spheres (~4 nm in diameter) with pure excitonic photoluminescence were continuously formed (Figure 3A), and the combined use of coaxial injection and H_2O_2 addition successfully addressed the clogging limitations encountered in most microfluidic application for chemical engineering.[51] Preparation of small-sized ZnO nanoparticles (7–26 nm) was also realized in a membrane dispersion microreactor (Figure 3B), where the use of NH_4HCO_3 fluid can generate CO_2 bubbles by the released heat from two-flow collision and precipitation processes for further intensifying

the mass transfer and reducing aggregation.[56] Through implementing a time pulsed mixing method (Figure 3C), microreactor was demonstrated to produce ZnO nanospheres with similar particle size (3–5 nm) and crystalline structure as batch reactor.[64] In addition, ultrasonic microreactor was also employed to synthesize green emission ZnO quantum dots with an average size of 2.4 nm (Figure 3D). Flow rate, ultrasonic power, and temperature significantly affected the type and quantity of defects in ZnO products.[70] These results demonstrate that ZnO spheres can be continuously synthesized from laminar flow microreactors or more complicated integrated microfluidic systems. However, the available particle sizes of these approaches were only in a narrow range from several to few tens of nanometers.

3.1.3 Flower—Continuous synthesis of ZnO flowers was generally carried out in laminar flow microreactors with a T-shaped mixer (Figure 4A).[47,59,63] The flower structures can be formed either on the oxidized silicon substrates[47,63] or in the solution base.[59] In the former approach, the size of ZnO flowers was found to be increased with increasing treatment time and temperature, and the structure of flowers was affected under different flow rates or concentrations of NaOH.[47,63] The latter solution growth approach not only allows controllable synthesis of ZnO flowers but also permits easy dopant addition. The resultant metals-doped ZnO flower structures exhibit much enhanced performance as a result of increased surface defect sites associated with oxygen when metals replace Zn in the crystal structure.[59] In addition to conventional glass capillary or PDMS microreactor, cellulose hydrogel with rich porous texture was also successfully employed as microreactor platform to synthesize ZnO flowers with relatively uniform particle size (Figure 4B).[74] These results validate the applicability of microfluidic reactors (even in a bioresource form) in the controllable synthesis of flower-like structures, providing new insights for the development of hierarchical ZnO products.

3.1.4 Sheet/flake—Microfluidic synthesis of ZnO sheet/flake nanostructures can be realized by two similar approaches as mentioned above: in-situ growth approach and ex-situ generation approach (Figure 5). Microfluidic in-situ growth approach not only permits oriented aligned nanosheets on the desired surface areas without any extra assembly process, but also allows additive reactants to be directly delivered to the pre-seeded reaction area with no or low reagents consumption (Figure 5A).[66] However, such approach only results in a localized reaction at the desired surface area, which limits the large scale fabrication of ZnO nanosheets. Comparatively, based on the serpentine and spiral microchannels (Figure 5B), ZnO nanosheets can be continuously collected from the outlet of microreactors at appropriate flow rates of zinc nitrate and sodium hydroxide fluids.[75,82] However, this ex-situ generation approach is hard to obtain aligned nanostructures in specific directions. Therefore, both approaches still face the challenge of grappling with the gap between controllable growth process and materials quality of ZnO sheets/flakes.

3.1.5 Spindle/ellipsoid—Continuous laminar flow synthesis of spindle/ellipsoid-like ZnO materials can be generally achieved by either self-assembly strategy[55,75,82] or seed-mediated growth strategy.[69] Microfluidic reaction system could not only facilitate the homogeneous nucleation and growth of ZnO nanocrystals by minimizing the temperature

and pH gradient in the solution, but also enable to tailor the crystal growth process by simply changing the operation parameters (such as flow rate and residence time). Relying on the Dean vortices in a winding microcapillary tube, ZnO spindles were successfully formed by the assembly of nanocrystals at an appropriate Dean number of 78 (Figure 6A), whereas non-assembled and spherical ZnO products were formed at Dean numbers of 36 and 150, respectively.[55] Similarly, PDMS-based Serpentine (Figure 6B) and spiral microchannels were also demonstrated to assemble spindles from ZnO nanocrystals but only at specific flow rates of reactant fluids.[75,82] In addition to self-assembly strategy, seed-mediated growth strategy was also developed for the flow synthesis of ZnO spindles in a continuous two-stage microfluidic system (Figure 6C). Monodispersed triangular silver nanoparticles were firstly formed in T-mixer and spiral microreactor, and then directly fed into cross-type mixer as seeds for the controllable growth of ZnO spindles on silver particle surface to form a final hedgehog-like Ag-ZnO structure.[69] These results demonstrate the feasibility of laminar flow microreactors in the synthesis of ZnO spindles, however, further studies that enable precise control of size dimensions of spindle/ellipsoid structures are necessary.

3.2 Discrete segmented flow synthesis

Compared to continuous laminar flow microreactors, discrete segmented flow microreactors have received very little attention from researchers for the synthesis of ZnO micro-/nanoparticles (Table 1). The reported discrete microreactors studies are mainly focused on the liquid-liquid segmented flow that generates droplets as water-in-oil emulsions (Figure 7).[52,62,77] The resultant droplets can serve as excellent reactors to carry out chemical reactions and form high quality ZnO products because of intensive mixing efficacy, consistent residence time, and efficient heat/mass transfer afforded by each droplet. T-junction (Figure 7A) and flow-focusing microfluidic device (Figure 7C) are usually designed to enable the droplet generation of reaction mixture in a continuous phase fluid.[52,77] In addition, droplet synthesis of ZnO materials could be also realized from microemulsions in a continuous flow microreactor (Figure 7B).[62] Many parameters can regulate the formation of the droplets, such as flow rate, solution viscosity, and microchannel geometry, which in turn affect the size and shape of ZnO particles. Liquid-gas segmented flow for the synthesis of ZnO particles has rarely been reported. One feasible way is to apply NH_4HCO_3 as reactant flow for the generation of CO_2 bubbles resulting from two-flow collision and precipitation processes in the reaction microchannel (Figure 3B),[56] and the other way is to integrate ultrasonic radiation with microreactor for bringing bubbles through ultrasonic cavitation (Figure 3D).[70] By choosing adequate precursors and reactants concentrations, sphere-, rod-, star-, and flower-shaped ZnO micro-/nanoparticles could be continuously produced from discrete flow microreactors,[52,62,77] and the particle sizes show more narrowly distribution than those from batch reactor.[62] These preliminary results pave the basis for exploring more rational design of discrete segmented flow microreactors in the controllable synthesis of ZnO materials.

4. Microfluidic applications of ZnO materials

In the past decade, microfluidic chips have demonstrated their great potentials in enabling micro-total analysis systems and integrating multiplexed functional units into a single

device. Given their advanced features such as high system integration, low sample consumption, fast response, good reproducibility, and high reliability, microfluidic chips have become attractive tools for many potential applications (Table 2). In this section, we will highlight the unprecedented opportunities of microchips in advancing applications of electrochemical sensing, immunofluorescent sensing, SERS sensing, biological separation, and molecular catalysis.

4.1 Electrochemical sensing

ZnO materials have fast electron transfer and high isoelectric point of 9.5 that can be electrostatically bonded to negatively charged matters at the physiological pH, while microfluidics enables high integration, fast response, and low sample consumption. These features endow microfluidics-ZnO as a promising platform for electrochemical sensing of targets such as pH,[53,94] biomolecules,[72,87,92,93,97] gas molecules,[65] and blood.[94,98] Since ZnO is an n-type semiconductor that could change its surface electron charge by the surrounding ion charge concentration, this change of surface charge causes electrical conductance modulation at different pH levels and thus allows for pH sensing. It was found that, due to the formation of a depletion layer at the surface, the conductance of ZnO nanowire array decreases as the pH level is increased.[53] Considering the slightly acidic extracellular environment of cancer cells at pH 6.2–6.9 compared to 7.3–7.4 of normal cells, highly sensitive and stable microfluidic pH sensor was developed for successfully identification of circulating tumor cells based on the precise pH measurements between ZnO working electrode and Ag/AgCl reference electrode (Figure 8A).[94] The integration of ZnO nanowires with microfluidic chip was also employed to measure the impedimetric ratio of erythrocytes to leukocytes for monitoring patient's disease activity (Figure 8B).[98] In addition, based on programmable temperature control and parallel chemical supply within microfluidic platform, heterogeneous ZnO-contained nanomaterial arrays were developed as multiplexed gas sensor for sub-ppm NO_2 and tens of ppm CO gas detection.[65] Similarly, ZnO-based PDMS and paper microfluidic chips have been widely applied for the sensing detection of various biomolecules, such as thyrotropin,[87] glucose,[92] IgG,[93] HIV p24 antigen,[93] amino acids (L-glutamic acid and L-cysteine),[97] and influenza viruses (H1N1, H5N1, and H7N9).[72] Specifically, PDMS microfluidic chip for electrochemical sensing of biomolecules generally involves both immobilized capture antibody and horseradish peroxidase (HRP)-conjugated detection antibody to generate a signal. HRP enables oxidation of its enzymatic substrate (such as 3,3',5,5'-tetramethylbenzidine[72] and 4-tert-butylcatechol[87]), resulting in both optical color change of substrate-containing solution and electrochemical redox current (Figure 8C). Comparatively, microfluidic paper-based analytical device (μPAD) integrated with ZnO materials represent a promising platform for label-free and ultrasensitive electrochemical detection due to its low cost, high portability, and ease of operation,[92,93,97] especially the unnecessary use of light-sensitive electron mediator for enhancing biosensing stability (Figure 8D). Among different types of ZnO materials, it is interesting to point out that flower-shaped nanostructure shows superior electrochemical signal compared to nanosphere, nanosheet, and nanorod arrays, revealing the importance of structural design when applying nanoparticles for biomedical applications.[99–103]

4.2 Immunofluorescent sensing

Due to their high specificity and sensitivity, immunofluorescent assays have been widely used in the sensing detection of biomolecules. Considering low sample consumption feature from microfluidics and desirable optical feature of wide band gap (3.37 eV) and large excitation binding energy (60 meV) from ZnO nanostructures, the integration of ZnO with microfluidics showed remarkable capability to improve the sensing performance of immunofluorescent assays. Almost all established immunofluorescent sensing studies utilized densely packed ZnO rods/wires with large surface-to-volume ratio and aspect ratio for greatly enhancing the fluorescent intensity.[71,78,80,88,96] Owing to their high transmittance and intrinsically enclosed microchannel, glass capillaries served as an ideal substrate for immunofluorescent sensing. When introducing polyacrylic acid (PAA) as a hydrophilic layer for increasing antibody loading capacity and reducing nonspecific protein adsorption, the resultant ZnO-PAA nanorod arrays constructed on the inner wall of glass capillaries can detect concentration of carcinoembryonic antigen (CEA) as low as 100 fg/mL (Figure 9A).[80] Besides glass capillaries, PDMS-based microfluidic chips have also been widely utilized for the immunofluorescent multiplex detection of proteins and virus.[71,78,96] ZnO nanowires-integrated microchannels can significantly lower down the detection limit to 1 pg/mL for α-fetoprotein (AFP) assay and 100 fg/mL for CEA assay (Figure 9B).[78] Particle shape has been revealed to affect the biological performance of nanomaterials,[104,105] it was also demonstrated to play significant roles in the immunofluorescent sensing detection of ZnO materials. Compared to rod nanowires and hexahedral-puncheon nanostructures, sharp ZnO nanowires exhibit the largest dynamic range and the highest fluorescent intensity.[71] When using the sharp nanowires for simultaneous anti-mouse IgG and anti-rabbit IgG detection, fluorescent images present clear multiple detections at the crossover areas (Figure 9C). In addition, ZnO nanorod array-integrated microfluidic chip can act as a multiplex immunofluorescent platform for highly selective and sensitive detection of avian influenza virus (AIV).[96] The unique optical property and 3D morphology of nanorod array allowed the detection limit of H5N2 AIV to as low as 3.6×10^3 EID_{50}/mL, which is around 22 times more sensitive than conventional enzyme-linked immunosorbent assay (Figure 9D). However, it is noted that native PDMS surfaces are hydrophobic and may adsorb small dye molecules, which may limit the applicability of PDMS in immunofluorescent analysis.[88]

4.3 SERS sensing

Label-free sensing detection of analytes from small volume, highly diluted, and multicomponent samples is vitally important in diverse fields. Surface-enhanced Raman scattering (SERS) technique allows direct, sensitive, nondestructive, and real-time record of quantitative chemical information, while microfluidic technique permits controllable manipulation of small volumes of fluids. Therefore, the integrated microfluidics-SERS platform represents a promising approach for label-free analysis of a small amount of analytes. In recent years, ZnO-based 3D nanostructured materials grown in microchannels have demonstrated to be effective in facilitating SERS detection of many analytes, such as protein, nucleic acid, dye, and cell (Figure 10).[61,67] By microfluidic in-situ deposition of Ag nanoparticles on the vertically aligned ZnO nanorods, the resultant Ag@ZnO as SERS substrate was able to detect 1 μM DNA and the surface chemical fingerprint of single living cell could be recorded (Figure 10A).[61] In addition, glass capillary-based SERS

microanalysis platforms were also developed because of their appealing features such as low cost, facile fabrication and operation, and special capillary forces that can readily drive fluid flowing into a capillary. Using afforded ZnO@ZnS-Ag clustered nanorod arrays on the inner wall of capillary microchannels, high SERS sensitivity of 4-mercaptobenzoic acid (4-MBA, 10^{-9} M), Rhodamine 6G (R6G, 10^{-9} M), and methylparathion (MP, 10^{-8} M) was achieved (Figure 10B).[67] Considering its simplicity, controllability, sensitivity, and versatility, ZnO-based microfluidics-SERS platform should be valuable in many biomedical and environmental applications.

4.4 Biological separation

Owing to its unique advantage of miniaturization and integration, microfluidics has drawn more and more attention in the field of biological separation. The integration of microfluidics with zinc oxide materials has successfully demonstrated its superior capabilities in the highly efficient enrichment of proteins[73,84] and cells.[95] Based on the coordination affinity of zinc to histidine, confined ZnO/Zn(OH)F nanowire arrays inside capillary microchannel could adsorb all the bovine hemoglobin (0.5 mg/mL) at the residence time of 50 s and isolate human hemoglobin from human blood (500-fold diluted) effectively due to high contact area afforded from 3D ZnO nanostructures.[73] Since phosphate functional groups can bind to the surface of metal oxide particles, TiO_2-immobilized ZnO nanorod arrays were also aligned on the inner wall of capillary microchannel for phosphopeptides enrichment from tryptic protein digests with great selectivity, sensitivity, and durability (Figure 11A).[84] In addition, to achieve highly efficient isolation and gently release of circulating tumor cells, microfluidic chip containing a wedge-shaped microchannel with gradually decreasing height and a layer of ZnO nanorods substrate was developed (Figure 11B). By integrating size-dependent filtration with degradable nanostructured substrate, the capture efficiency over 87.5% was achieved and up to 85.6% of the captured cells were easily released after reverse injection of diluted phosphoric acid to dissolve ZnO substrate.[95] Given their superior features, microfluidics-integrated ZnO materials may find more great success in the separation of a large variety of biomolecules and cells.

4.5 Molecular catalysis

Microfluidic chips have attracted great attention for catalysis applications due to their inherently large surface-to-volume ratio, short diffusion distance, rapid mass transfer, and high integration capabilities. By easy interfacing with UV light, microchips find great niches in photocatalysis for the photodegradation of methylene blue (MB),[50,60,73] phenol,[85] methyl orange,[76] and volatile organic compounds (Benzene, Toluene, Ethylbenzene, m–p Xylenes, and o-Xylene).[79] ZnO nanowires have high electron transfer rate and could be grown on a patterned area over a glass substrate[60,76] (Figure 12A) or Si substrate[79] (Figure 12B), allowing easy integration into chamber-based microfluidic chips.[60,76,79] Besides microchamber, ZnO wire/rod arrays could be also patterned on the inner wall of glass capillary-based microfluidic chips for continuous flow photocatalysis (Figures 12C–D).[50,73,85] Given that one of the major issues for ZnO photocatalysts is the lower photocatalytic efficiency due to quick combination of photoinduced charge carriers, many heterostructures, such as TiO_2-coated ZnO rod arrays[50] (Figure 12C) and Pt-coated ZnO rod arrays[85] (Figure 12D), were developed inside the capillary microchannel. These kinds of hetero-

photocatalysts not only suppressed the recombination of photogenerated electron-hole pairs, but also extended the light adsorption spectrum and thus improved the light use efficiency.[50,85] It is noted that, in addition to photocatalysis, microfluidic chips with integrated ZnO-based hetero-catalysts also exhibit superior performance in the direct conversion of syngas to dimethyl ether and methanol.[81,91] These results clearly reflect the robust applicability of microfluidics-ZnO as catalysis systems, especially in the photocatalysis field. Although considerable progress has been achieved, the greatest challenge facing microfluidic chips is the throughput when applying ZnO catalysts into practical industrial settings.

Besides the bioapplication areas discussed above, ZnO materials also enable some other promising applications established with microfluidic systems. ZnO thin film-based surface acoustic wave (SAW) devices have been successfully utilized to fabricate microfluidic pumps.[83,86,89,90] Among different deposition substrates (Si, glass, and polyimide), ZnO deposited on Si substrate exhibit the highest acoustic streaming velocity of about 10 cm/s and the shortest particle concentration time of less than 10 seconds.[90] When introducing ultra-smooth nanocrystalline diamond films with high-acoustic wave velocity as interlayer into ZnO-based SAW device, microfluidic efficiency was found to be further enhanced due to reduced acoustic energy dissipation into Si substrate and improved acoustic properties of SAW devices.[86] In addition, by patterning ZnO nanowire arrays as special U-shaped microcages, microparticles were trapped while the dispersion media continuously flew out through the porous network of nanowires, revealing their great potential as single cell capture structures.[53] Another interesting application is for facile and high-throughput mechanical cell lysis by virtue of the sharp ends of high aspect ratios of nanowires. Microfluidic chip integrated with patterned ZnO nanowire array was demonstrated to successfully tear the plasma membrane, which is even more effective than conventional chemical lysis methods but with shorter processing time and simpler equipment.[54] Furthermore, due to their superior features such as ease of synthesis, low cost, wide bandgap, high bulk electron mobility, appropriate refractive index, and flexible morphology control, ZnO nanostructures have already demonstrated their great potential in energy-harvesting devices.[57,66]

5. Current challenges and future perspectives

The past decade has witnessed considerable progress in the development of microfluidic systems for controllable synthesis and applications of ZnO micro-/nanomaterials. Owing to their many unique and attractive features (especially flexible spatio-temporal control, high integration capability, and low samples consumption),[106–113] microfluidic devices fabricated with PDMS or glass capillary significantly advance the rational design and applicability of functional materials. To date, ZnO structures with different sizes, shapes, and compositions have been developed for applications in biomedical fields. However, many challenges still remain to be addressed before the full potential of microfluidics can be realized.

From the materials synthesis aspect, 1) compared to conventional batch reactors, microfluidic reactors provide new and alternative opportunities for controllable synthesis of ZnO materials. However, only very few studies revealed the unique merits of microreactors by direct comparison to batch reactors at the same reaction conditions.[49,63,64,68] More

parallel studies are greatly needed to demonstrate the advanced features of microfluidics for ZnO production in terms of faster reaction kinetics, higher reproducibility, and better physicochemical properties. 2) there is still a lack of inline management control over flow synthesis process. Full exploitation of microfluidic systems requires real-time information about the chemical reaction progress for realizing an immediate response in the optimization of structural properties. Although microreactors permit high integration and automation, inline control systems for ZnO materials synthesis are still rarely reported. 3) despite ZnO materials with different sizes (from few nanometers to tens of micrometers), shapes (wire/rod, sphere, flower, sheet/flake, and spindle/ellipsoid), and compositions (such as metal-doped, polymer-modified, and functional nanoparticles-coated) are already available from microreactors, there is still relatively low structural diversity. As shown in Table 1, most ZnO particles are sizes less than ten nanometers or larger than submicrometer, mainly wire/rod and sphere shapes, and lack of variability in hierarchical compositions. To meet the needs of diverse applications, ZnO materials with rich structural diversity should be systematically developed. 4) due to small dimensions and low operation volumes of microreactors, the production amount of ZnO materials can only achieve up to grams per day.[82] To further improve the yields, more robust and integrated design of microreactors with parallel multiple modules should be established for scale-up production of ZnO materials.

From the materials application aspect, 1) given unique advantages of microfluidic chips, plenty of studies on the integration of ZnO materials with microfluidics has been carried out and achieved significant progress in the areas of biosensing, biological separation, and molecular catalysis (Table 2). Though many ZnO-based PDMS and glass capillary microfluidic devices have been developed and exhibited good performance, the applications of ZnO materials in microfluidic chips is still in urgent need of being optimized and improved.[73] 2) almost all the established microfluidic application systems relied on the nanowire or nanorod array of ZnO materials, comparatively, very little attention has been paid for exploring other structures. Although it can be easily understood that the in-situ deposited wire/rod array inside microchannel provides great convenience for subsequent analysis and application, the structural properties of ZnO materials should be systematically investigated to fully reveal their potential use. 3) the effect of particle structures (such as particle size and shape) on the application performance of ZnO materials is still rarely examined in microfluidic systems.[82,97] Since a large number of studies have already shown that particle structures of micro-/nanomaterials significantly regulate their downstream application efficacy,[114–117] more attention should be paid to maximizing the potential of ZnO materials. 4) most of the ZnO-integrated microfluidic application systems are still in the proof-of-concept stage. Compared to conventional batch operation systems, microfluidic chips have demonstrated superior performance in sensing sensitivity, separation capability, and catalysis efficiency. However, one of the biggest challenges facing microfluidic application systems is how to improve the throughput while keeping the same efficient performance inside miniaturized devices. Therefore, there still has a long way to go from laboratory benches to practical implementation in industrial settings.

6. Conclusion

This review provides a comprehensive summary of recent advances in microfluidics-enabled rational design, controllable synthesis and on-chip applications of ZnO micro-/nanomaterials. We discussed the flow synthesis approaches of ZnO materials with different structures (wire, rod, sphere, flower, sheet, flake, spindle, and ellipsoid) using continuous laminar flow microreactors and discrete segmented flow microreactors, and highlighted the unprecedented opportunities for applying ZnO-integrated microchips in biosensing, biological separation, and molecular catalysis applications, and finally pointed out the major challenges and opportunities for inspiring future studies in this area. Despite great achievement in a relatively short period, microfluidics is still a less exploited tool in the synthesis and applications of ZnO structures. Given that researchers from different disciplines are attracted and start to explore the advances of microfluidics, it will open up a new frontier for functional materials development and will definitely impact various application areas.

Acknowledgement

The authors are grateful for the financial support from the National Institute of Health (NIH) Director's Transformative Research Award (R01HL137157), NSF ECCS-1509369, and Norris Cotton Cancer Center Developmental Funds (Pilot Projects).

Reference

1. Rahman F, Opt. Eng, 2019, 58, 010901.
2. Vittal R and Ho KC, Renew. Sust. Energ. Rev, 2017, 70, 920–935.
3. Mishra PK, Mishra H, Ekielski A, Talegaonkar S and Vaidya B, Drug Discov. Today, 2017, 22, 1825–1834. [PubMed: 28847758]
4. Lee KM, Lai CW, Ngai KS and Juan JC, Water Res, 2016, 88, 428–448. [PubMed: 26519627]
5. Wang ZL, J. Phys. Condens. Matter, 2004, 16, R829–R858.
6. Moezzi A, McDonagh AM and Cortie MB, Chem. Eng. J, 2012, 185–186, 1–22.
7. Whitesides GM, Nature, 2006, 442, 368–373. [PubMed: 16871203]
8. Song H, Chen DL and Ismagilov RF, Angew. Chem. Int. Ed, 2006, 45, 7336–7356.
9. Abou-Hassan A, Sandre O and Cabuil V, Angew. Chem. Int. Ed, 2010, 49, 6268–6286.
10. Teh S-Y, Lin R, Hung L-H and Lee AP, Lab Chip, 2008, 8, 198–220. [PubMed: 18231657]
11. Hung LH and Lee AP, J. Med. Biol. Eng, 2007, 27, 1–6.
12. Song Y, Hormes J and Kumar CSSR, Small, 2008, 4, 698–711. [PubMed: 18535993]
13. Singh A, Malek CK and Kulkarni SK, Int. J. Nanosci, 2010, 9, 93–112.
14. Marre S and Jensen KF, Chem. Soc. Rev, 2010, 39, 1183–1202. [PubMed: 20179831]
15. Wang J-T, Wang J and Han J-J, Small, 2011, 7, 1728–1754. [PubMed: 21618428]
16. Pumera M, Chem. Commun, 2011, 47, 5671–5680.
17. Zhao C-X, He L, Qiao SZ and Middelberg APJ, Chem. Eng. Sci, 2011, 66, 1463–1479.
18. Knauer A and Koehler JM, Nanotechnol. Rev, 2014, 3, 5–26.
19. Kim JH, Jeon TY, Choi TM, Shim TS, Kim SH and Yang SM, Langmuir, 2014, 30, 1473–1488. [PubMed: 24143936]
20. Hao N, Nie Y and Zhang JXJ, Int. Mater. Rev, 2018, 63, 461–487.
21. Yu B, Lee RJ and Lee LJ, in Methods in Enzymology, 2009, vol. 465, pp. 129–141. [PubMed: 19913165]
22. Dendukuri D and Doyle PS, Adv. Mater, 2009, 21, 4071–4086.

23. Il Park J, Saffari A, Kumar S, Günther A and Kumacheva E, Annu. Rev. Mater. Res, 2010, 40, 415–443.
24. Chung BG, Lee K-H, Khademhosseini A and Lee S-H, Lab Chip, 2012, 12, 45–59. [PubMed: 22105780]
25. Capretto L, Carugo D, Mazzitelli S, Nastruzzi C and Zhang X, Adv. Drug Deliv. Rev, 2013, 65, 1496–1532. [PubMed: 23933616]
26. Wang W, Zhang M-J and Chu L-Y, Acc. Chem. Res, 2014, 47, 373–384. [PubMed: 24199893]
27. Baah D and Floyd-Smith T, Microfluid. Nanofluid, 2014, 17, 431–455.
28. Shahbazali E, Hessel V, Noël T and Wang Q, Nanotechnol. Rev, 2014, 3, 65–86.
29. Rahman M and Rebrov E, Processes, 2014, 2, 466–493.
30. Nightingale AM and de Mello JC, J. Mater. Chem, 2010, 20, 8454–8463.
31. Phillips TW, Lignos IG, Maceiczyk RM, DeMello AJ and DeMello JC, Lab Chip, 2014, 14, 3172–3180. [PubMed: 24911190]
32. Hao N and Zhang JXJ, Biomicrofluidics, 2019, 13, 051501.
33. Hao N, Nie Y and Zhang JXJ, Biomater. Sci, 2019, 7, 2218–2240. [PubMed: 30919847]
34. Badilescu S and Packirisamy M, Polymers (Basel)., 2012, 4, 1278–1310.
35. Boken J, Soni SK and Kumar D, Crit. Rev. Anal. Chem, 2016, 46, 538–561. [PubMed: 27070948]
36. Hao N, Nie Y, Xu Z, Jin C, Fyda TJ and Zhang JXJ, J. Colloid Interf. Sci, 2020, 559, 254–262.
37. Zhao C-X, Adv. Drug Deliv. Rev, 2013, 65, 1420–1446. [PubMed: 23770061]
38. Björnmalm M, Yan Y and Caruso F, J. Control. Release, 2014, 190, 139–149. [PubMed: 24794898]
39. Khan IU, a Serra C, Anton N and Vandamme TF, Expert Opin. Drug Deliv, 2014, 12, 1–16. [PubMed: 25169007]
40. Riahi R, Tamayol A, Shaegh SAM, Ghaemmaghami AM, Dokmeci MR and Khademshosseini A, Curr. Opin. Chem. Eng, 2015, 7, 101–112. [PubMed: 31692947]
41. Valencia PM, Farokhzad OC, Karnik R and Langer R, Nat. Nanotechnol, 2012, 7, 623–629. [PubMed: 23042546]
42. Feng Q, Sun J and Jiang X, Nanoscale, 2016, 8, 12430–12443. [PubMed: 26864887]
43. Ma J, Lee SM-Y, Yi C and Li C-W, Lab Chip, 2017, 17, 209–226. [PubMed: 27991629]
44. Zhao X, Bian F, Sun L, Cai L, Li L and Zhao Y, Small, 2019, 1, 1901943.
45. Ren K, Zhou J and Wu H, Acc. Chem. Res, 2013, 46, 2396–2406. [PubMed: 24245999]
46. Sue K, Kimura K and Arai K, Mater. Lett, 2004, 58, 3229–3231.
47. Jung JY, Park N-K, Han S-Y, Han GB, Lee TJ, Ryu SO and Chang C-H, Curr. Appl. Phys, 2008, 8, 720–724.
48. McPeak KM and Baxter JB, Cryst. Growth Des, 2009, 9, 4538–4545.
49. McPeak KM and Baxter JB, Ind. Eng. Chem. Res, 2009, 48, 5954–5961.
50. He Z, Li Y, Zhang Q and Wang H, Appl. Catal. B, 2010, 93, 376–382.
51. Roig Y, Marre S, Cardinal T and Aymonier C, Angew. Chem. Int. Ed, 2011, 50, 12071–12074.
52. Li S, Gross GA, Günther PM and Köhler JM, Chem. Eng. J, 2011, 167, 681–687.
53. Kim J, Li Z and Park I, Lab Chip, 2011, 11, 1946. [PubMed: 21499615]
54. Kim J, Hong JW, Kim DP, Shin JH and Park I, Lab Chip, 2012, 12, 2914. [PubMed: 22722645]
55. Choi C-H, Su Y-W and Chang C, CrystEngComm, 2013, 15, 3326.
56. Huang C, Wang Y and Luo G, Ind. Eng. Chem. Res, 2013, 52, 5683–5690.
57. Mehare RS, Devarapalli RR, Yenchalwar SG and Shelke MV, Microfluid. Nanofluid, 2013, 15, 1–9.
58. Ladanov M, Algarin-Amaris P, Matthews G, Ram M, Thomas S, Kumar A and Wang J, Nanotechnology, 2013, 24, 375301. [PubMed: 23965410]
59. Kim K-J, Kreider PB, Choi C, Chang C-H and Ahn H-G, RSC Adv, 2013, 3, 12702.
60. Han Z, Li J, He W, Li S, Li Z, Chu J and Chen Y, Microelectron. Eng, 2013, 111, 199–203.

61. Xie Y, Yang S, Mao Z, Li P, Zhao C, Cohick Z, Huang P-H and Huang TJ, ACS Nano, 2014, 8, 12175–12184. [PubMed: 25402207]
62. Wang Y, Zhang X, Wang A, Li X, Wang G and Zhao L, Chem. Eng. J, 2014, 235, 191–197.
63. Choi C-H and Chang C, Cryst. Growth Des, 2014, 14, 4759–4767.
64. Kang HW, Leem J, Yoon SY and Sung HJ, Nanoscale, 2014, 6, 2840–2846. [PubMed: 24469327]
65. Yang D, Kang K, Kim D, Li Z and Park I, Sci. Rep, 2015, 5, 8149. [PubMed: 25634814]
66. Zhao C, Zhang J, Hu Y, Robertson N, Hu PA, Child D, Gibson D and Fu YQ, Sci. Rep, 2015, 5, 17750. [PubMed: 26631685]
67. Wang G, Li K, Purcell FJ, Zhao D, Zhang W, He Z, Tan S, Tang Z, Wang H and Reichmanis E, ACS Appl. Mater. Interfaces, 2016, 8, 24974–24981. [PubMed: 27585300]
68. Choi CH, Levin JB and Chang CH, CrystEngComm, 2016, 18, 8645–8652.
69. Tao S, Yang M, Chen H, Ren M and Chen G, RSC Adv, 2016, 6, 45503–45511.
70. Yang W, Yang H, Ding W, Zhang B, Zhang L, Wang L, Yu M and Zhang Q, Ultras. Sonochem, 2016, 33, 106–117.
71. Sang C-H, Chou S-J, Pan FM and Sheu J-T, Biosens. Bioelectron, 2016, 75, 285–292. [PubMed: 26322591]
72. Han J-H, Lee D, Chew CHC, Kim T and Pak JJ, Sensor. Actuat. B, 2016, 228, 36–42.
73. Zhao D, He Z, Wang G, Wang H, Zhang Q and Li Y, Sensor. Actuat. B, 2016, 229, 281–287.
74. Qin C, Li S, Jiang G, Cao J, Guo Y, Li J, Zhang B and Han S, BioResources, 2017, 12, 3182–3191.
75. Baruah A, Jindal A, Acharya C, Prakash B, Basu S and Ganguli AK, J. Micromech. Microeng, 2017, 27, 035013.
76. Zhao P, Qin N, Wen JZ and Ren CL, Appl. Catal. B, 2017, 209, 468–475.
77. Stolzenburg P, Lorenz T, Dietzel A and Garnweitner G, Chem. Eng. Sci, 2018, 191, 500–510.
78. Guo L, Shi Y, Liu X, Han Z, Zhao Z, Chen Y, Xie W and Li X, Biosens. Bioelectron, 2018, 99, 368–374. [PubMed: 28802749]
79. Azzouz I, Habba YG, Capochichi-Gnambodoe M, Marty F, Vial J, Leprince-Wang Y and Bourouina T, Microsys. Nanoeng, 2018, 4, 17093.
80. Wu Z, Zhao D, Hou C, Liu L, Chen J, Huang H, Zhang Q, Duan Y, Li Y and Wang H, Nanoscale, 2018, 10, 17663–17670. [PubMed: 30206611]
81. Jiang X, Chen X, Ling C, Chen S and Wu Z, Appl. Catal. A, 2019, 570, 192–199.
82. Hao N, Xu Z, Nie Y, Jin C, Closson AB, Zhang M and Zhang JXJ, Chem. Eng. J, 2019, 378, 122222. [PubMed: 32831625]
83. Du XY, Fu YQ, Luo JK, Flewitt AJ and Milne WI, J. Appl. Phys, 2009, 105, 024508.
84. He Z, Zhang Q, Wang H and Li Y, Biomed. Microdevices, 2011, 13, 865–875. [PubMed: 21698384]
85. Zhang Q, Zhang Q, Wang H and Li Y, J. Hazard. Mater, 2013, 254–255, 318–324.
86. Pang HF, Fu YQ, Garcia-Gancedo L, Porro S, Luo JK, Placido F, Wilson JIB, Flewitt AJ, Milne WI and Zu XT, Microfluid. Nanofluid, 2013, 15, 377–386.
87. Seia MA, Pereira SV, Fernández-Baldo MA, De Vito IE, Raba J and Messina GA, Anal. Bioanal. Chem, 2014, 406, 4677–4684. [PubMed: 24908405]
88. Habouti S, Kunstmann-Olsen C, Hoyland JD, Rubahn HG and Es-Souni M, Appl. Phys. A, 2014, 115, 645–649.
89. Guo YJ, Lv HB, Li YF, He XL, Zhou J, Luo JK, Zu XT, Walton AJ and Fu YQ, J. Appl. Phys, 2014, 116, 024501.
90. Wang W, He X, Zhou J, Gu H, Xuan W, Chen J, Wang X and Luo JK, J. Electrochem. Soc, 2014, 161, B230–B236.
91. Allahyari S, Haghighi M and Ebadi A, Chem. Eng. J, 2015, 262, 1175–1186.
92. Li X, Zhao C and Liu X, Microsys. Nanoeng, 2015, 1, 1–7.
93. Li X and Liu X, Adv. Heal. Mater, 2016, 5, 1326–1335.
94. Mani GK, Morohoshi M, Yasoda Y, Yokoyama S, Kimura H and Tsuchiya K, ACS Appl. Mater. Interfaces, 2017, 9, 5193–5203. [PubMed: 28117972]

95. Li S, Gao Y, Chen X, Qin L, Cheng B, Wang S, Wang S, Zhao G, Liu K and Zhang N, Biomed. Microdevices, 2017, 19, 93. [PubMed: 29071494]
96. Yu X, Xia Y, Tang Y, Zhang W-L, Yeh Y-T, Lu H and Zheng S-Y, Small, 2017, 13, 1700425.
97. Kong Q, Wang Y, Zhang L, Xu C and Yu J, Biosens. Bioelectron, 2018, 110, 58–64. [PubMed: 29602031]
98. Weng K-Y, Chang Y-J, Ho C-Y, Liou DU, Huang Y-T, Chung W-Y and Chin T-Y, J. Med. Biol. Eng, 2018, 38, 150–158.
99. Nel AE, Mädler L, Velegol D, Xia T, V Hoek EM, Somasundaran P, Klaessig F, Castranova V and Thompson M, Nat. Mater, 2009, 8, 543–557. [PubMed: 19525947]
100. Hao N, Li LF and Tang FQ, J. Mater. Chem. A, 2014, 2, 11565–11568.
101. Hao NJ, Jayawardana KW, Chen X and Yan M, ACS Appl. Mater. Interfaces, 2015, 7, 1040–1045. [PubMed: 25562524]
102. Albanese A, Tang PS and Chan WCW, Annu. Rev. Biomed. Eng, 2012, 14, 1–16. [PubMed: 22524388]
103. Hao N, Chen X, Jayawardana KW, Wu B, Sundhoro M and Yan M, Biomater. Sci, 2016, 4, 87–91. [PubMed: 26364920]
104. Hao N, Li L and Tang F, Biomater. Sci, 2016, 4, 575–591. [PubMed: 26818852]
105. Hao N, Li LF and Tang FQ, Int. Mater. Rev, 2017, 62, 57–77.
106. Hao N, Nie Y, Tadimety A, Closson AB and Zhang JXJ, Mater. Res. Lett, 2017, 5, 584–590. [PubMed: 30854261]
107. Hao N, Nie Y, Tadimety A, Shen T and Zhang JXJ, Biomater. Sci, 2018, 6, 3121–3125. [PubMed: 30375583]
108. Hao N, Nie Y, Shen T and Zhang JXJ, Lab Chip, 2018, 18, 1997–2002. [PubMed: 29923569]
109. Hao N and Zhang JXJ, Sep. Purif. Rev, 2018, 47, 19–48.
110. Hao N, Nie Y and Zhang JXJ, ACS Sustain. Chem. Eng, 2018, 6, 1522–1526.
111. Hao N, Nie Y, Closson AB and Zhang JXJ, J. Colloid Interf. Sci, 2019, 539, 87–94.
112. Hao N, Nie Y, Xu Z, Closson AB, Usherwood T and Zhang JXJ, Chem. Eng. J, 2019, 366, 433–438. [PubMed: 31762686]
113. Hao N, Nie Y, Xu Z and Zhang JXJ, J. Colloid Interf. Sci, 2019, 542, 370–378.
114. Huang X, Li L, Liu T, Hao N, Liu H, Chen D and Tang F, ACS Nano, 2011, 5, 5390–5399. [PubMed: 21634407]
115. Yang K and Ma YQ, Nat. Nanotechnol, 2010, 5, 579–583. [PubMed: 20657599]
116. Petros RA and Desimone JM, Nat. Rev. Drug Discov, 2010, 9, 615–627. [PubMed: 20616808]
117. Geng Y, Dalhaimer P, Cai SS, Tsai R, Tewari M, Minko T and Discher DE, Nat. Nanotechnol, 2007, 2, 249–255. [PubMed: 18654271]

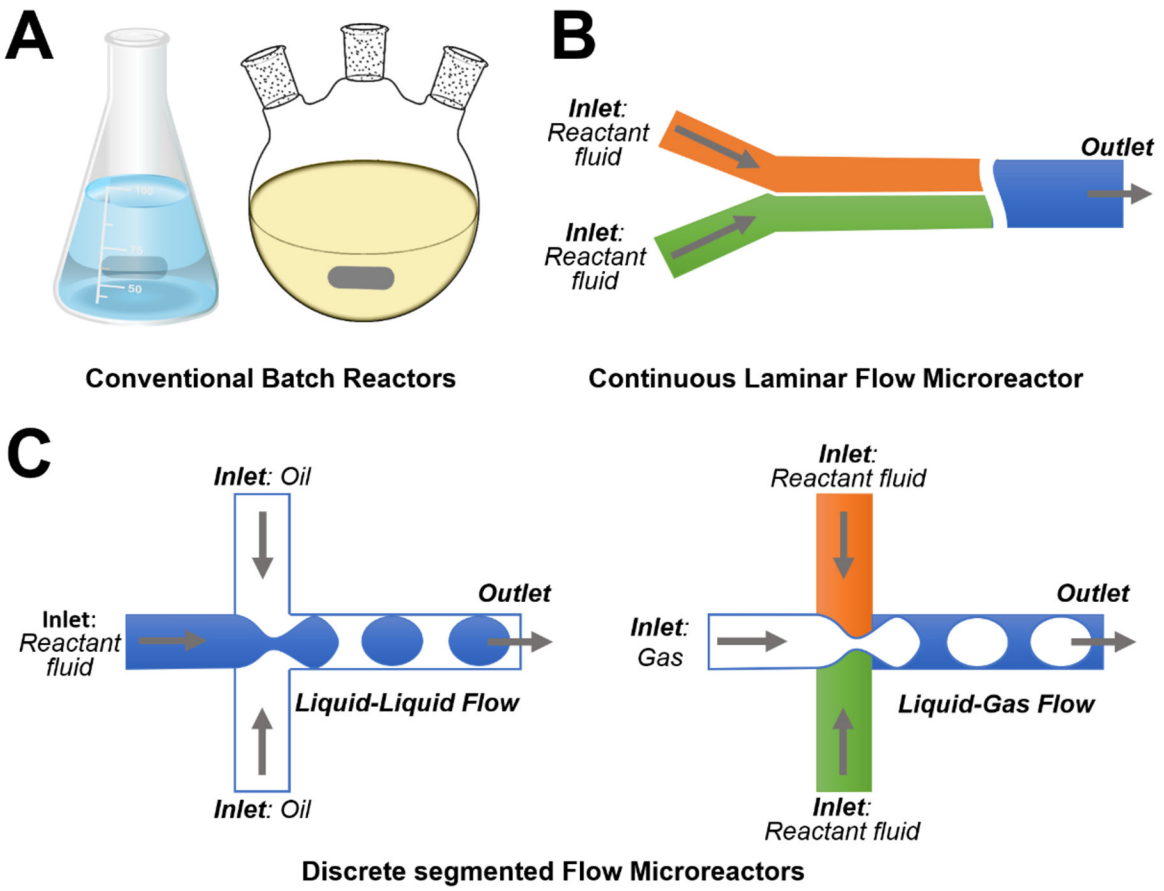

Figure 1:

Schematic illustrations showing examples of different types of reactors: (A) conventional batch reactors; (B) continuous laminar flow microreactor; and (C) discrete segmented flow microreactors.

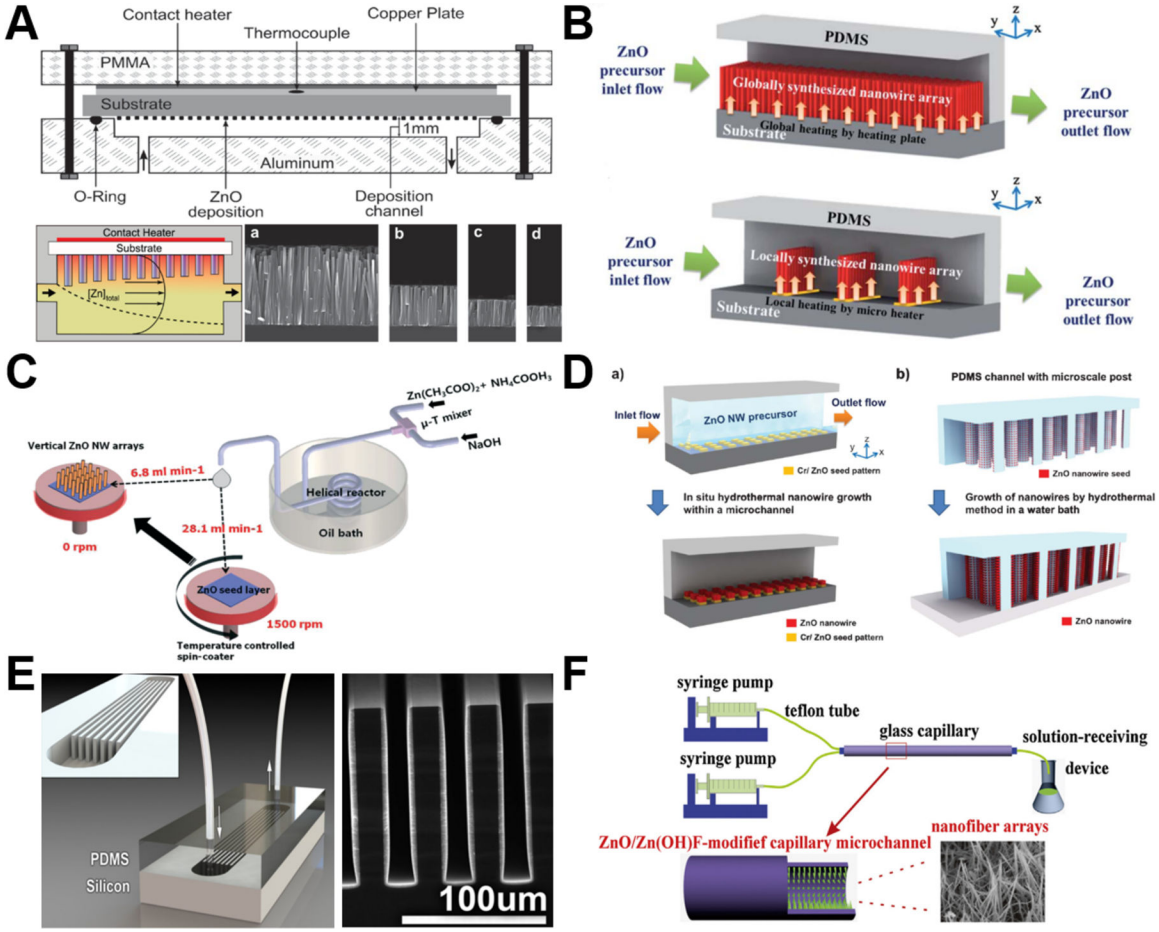

Figure 2.

Continuous laminar flow microreactors for the synthesis of wire/rod-like ZnO materials. (A) ZnO Nanowires grown by chemical bath deposition in a continuous flow microreactor (a, b, c, and d SEM images were taken at positions downstream from the inlet). Reproduced with permissions from reference[48], copyright 2009, American Chemical Society. (B) Schematics of in-situ synthesis and integration of ZnO nanowires in microfluidic chip: (top) global synthesis in the entire fluidic channel and (bottom) local synthesis by microheaters in the fluidic channel. Reproduced with permissions from reference[53], copyright 2011, Royal Society of Chemistry. (C) Schematic diagram showing the growth of the seed layer and vertical ZnO nanowire arrays using the microreactor-assisted nanoparticle deposition system. Reproduced with permissions from reference[68], copyright 2016, Royal Society of Chemistry. (D) Schematic diagram of (a) patterned growth of ZnO nanowire arrays by an in situ synthesis method and (b) growth of ZnO nanowires on microstructure arrays by a conventional hydrothermal method. Reproduced with permissions from reference[54], copyright 2012, Royal Society of Chemistry. (E) Microfluidic hydrothermal growth of ZnO nanowires over high aspect ratio microstructures. Reproduced with permissions from reference[58], copyright 2013, IOP Publishing, Ltd. (F) Schematic diagram of the synthesis of the ZnO/Zn(OH)F nanofiber array constructed on the inner wall of capillary microchannel. Reproduced with permissions from reference[73], copyright 2016, Elsevier.

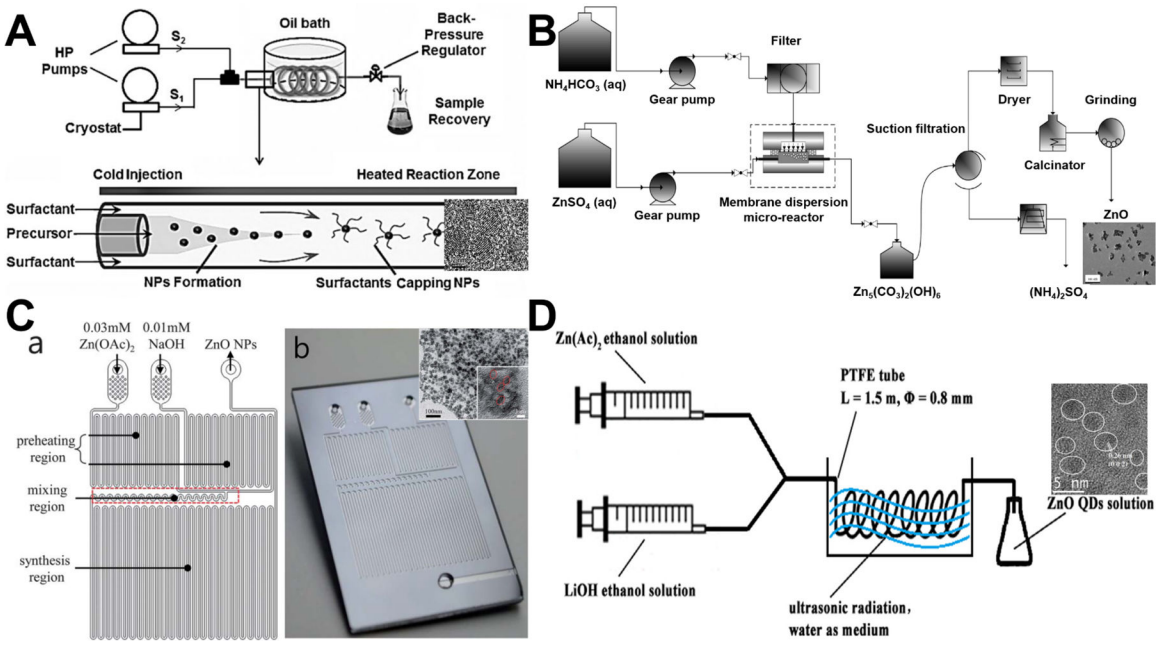

Figure 3.

Continuous laminar flow microreactors for the synthesis of sphere-like ZnO materials. (A) Synthesis of exciton luminescent ZnO nanocrystals using continuous supercritical microfluidics. Reproduced with permissions from reference[51], copyright 2011, John Wiley & Sons. (B) Preparation of small-sized ZnO nanoparticles in a membrane dispersion microreactor. Reproduced with permissions from reference[56], copyright 2013, American Chemical Society. (C) Schematic diagram (a) and photograph (b) of the microfluidic channel with time pulsed mixing used for ZnO nanoparticles synthesis. Reproduced with permissions from reference[64], copyright 2014, Royal Society of Chemistry. (D) Synthesis of high quantum yield ZnO quantum dots via an ultrasonication microreactor method. Reproduced with permissions from reference[70], copyright 2016, Elsevier.

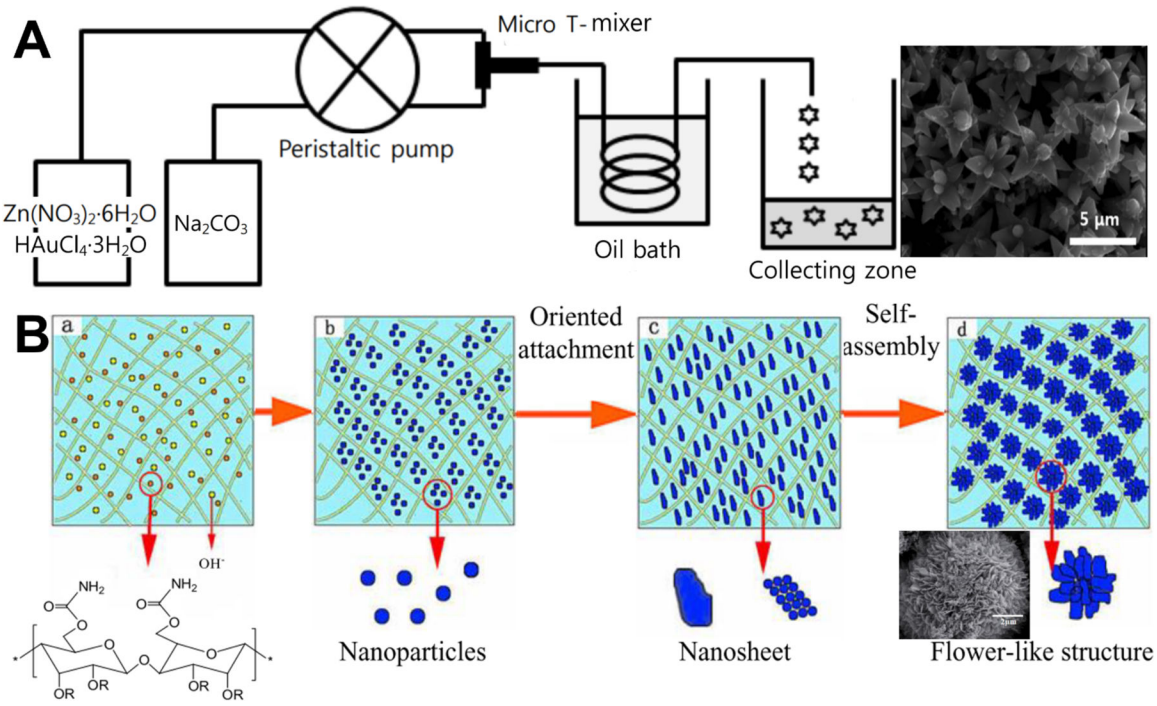

Figure 4.

Continuous laminar flow microreactors for the synthesis of flower-like ZnO materials. (A) Schematic diagram of T-shaped micromixer reactor system for the synthesis of ZnO microflower. Reproduced with permissions from reference[59], copyright 2013, Royal Society of Chemistry. (B) Preparation of flower-like ZnO nanoparticles in a cellulose hydrogel microreactor. Reproduced with permissions from reference[74], copyright 2017, North Carolina University.

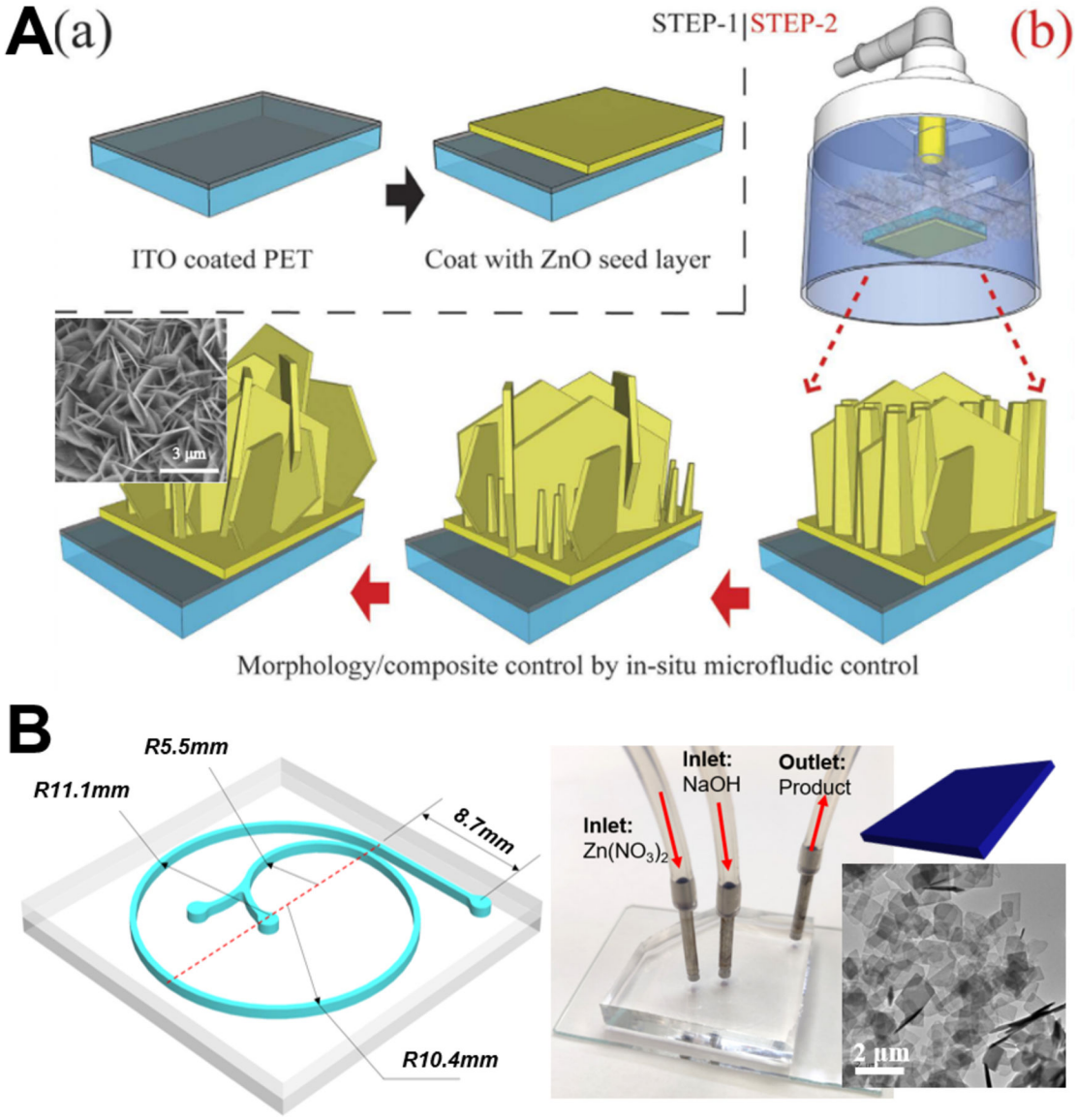

Figure 5.

Continuous laminar flow microreactors for the synthesis of sheet-like ZnO materials. (A) Illustration of the strategy for fabrication of controllable Al-doped ZnO (AZO) nanostructures: (a) step 1 for pre-seed substrates; (b) step 2 for in-situ hydrothermal method used for controllable AZO synthesis. Reproduced with permissions from reference[66], copyright 2015, Springer Nature. (B) Spiral-shaped laminar flow microreactor for the synthesis of ZnO nanosheet. Reproduced with permissions from reference[82], copyright 2019, Elsevier.

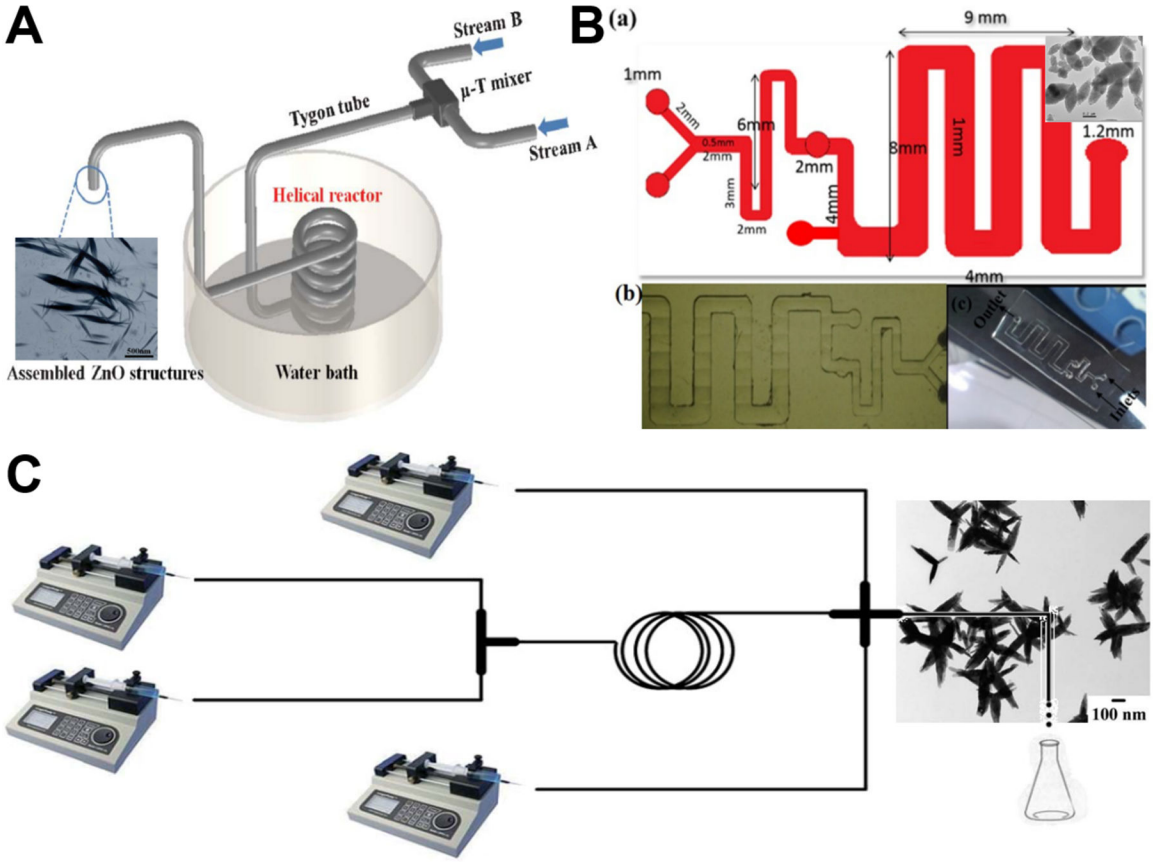

Figure 6.

Continuous laminar flow microreactors for the synthesis of spindle-like ZnO materials. (A) Schematic diagram of the growth and assembly of ZnO tactoids in a continuous flow microreactor. Reproduced with permissions from reference[55], copyright 2013, Royal Society of Chemistry. (B) PDMS-based microreactor for the synthesis of ZnO spindles. Reproduced with permissions from reference[75], copyright 2017, IOP Publishing, Ltd. (C) Experimental setup used for the continuous preparation of Ag–ZnO nanohedgehog. Reproduced with permissions from reference[69], copyright 2016, Royal Society of Chemistry.

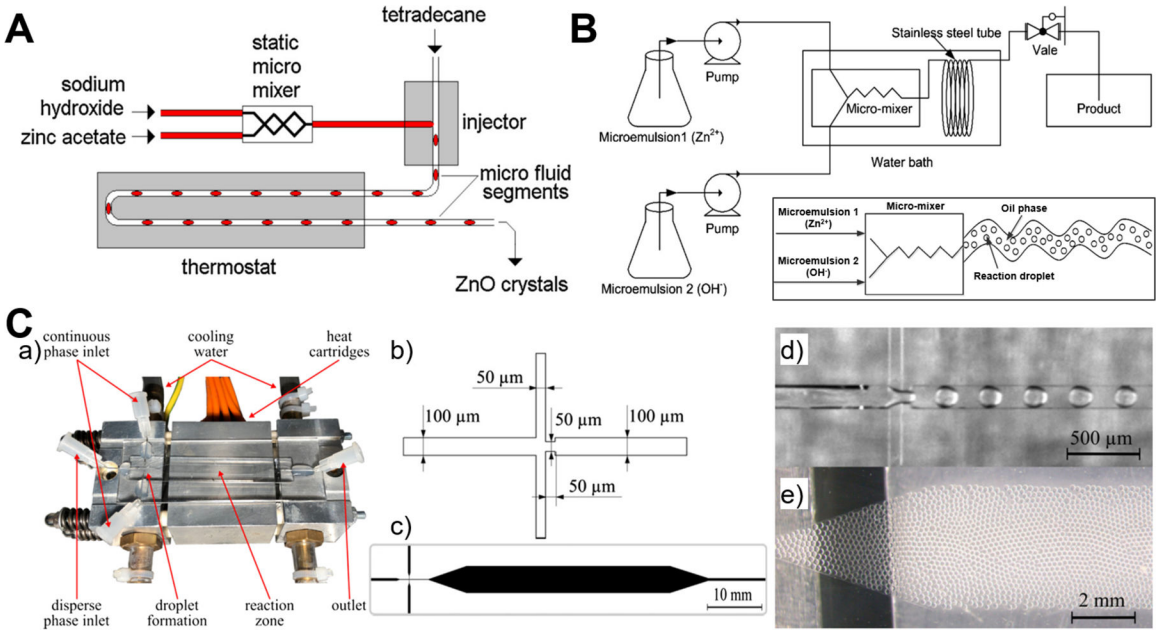

Figure 7.

Discrete segmented flow microreactors for the synthesis of ZnO materials. (A) Experimental setup for hydrothermal continuous-flow synthesis of sphere-, cylinder-, star- and flower-like ZnO microparticles. Reproduced with permissions from reference[52], copyright 2011, Elsevier. (B) Schematic diagram for the flow synthesis of nanoparticles by microemulsion in a microreactor. Reproduced with permissions from reference[62], copyright 2014, Elsevier. (C) Microfluidic droplet synthesis of ZnO nanoparticles: (a) Photograph of microfluidic chip; (b) Flow-focusing geometry; (c) Microfluidic design with expansion channel in the heated reaction zone; (d) Droplet formation of precursor and benzyl alcohol in Fluoronox; (e) Stable and monodisperse droplets in the reaction zone of the device. Reproduced with permissions from reference[77], copyright 2018, Elsevier.

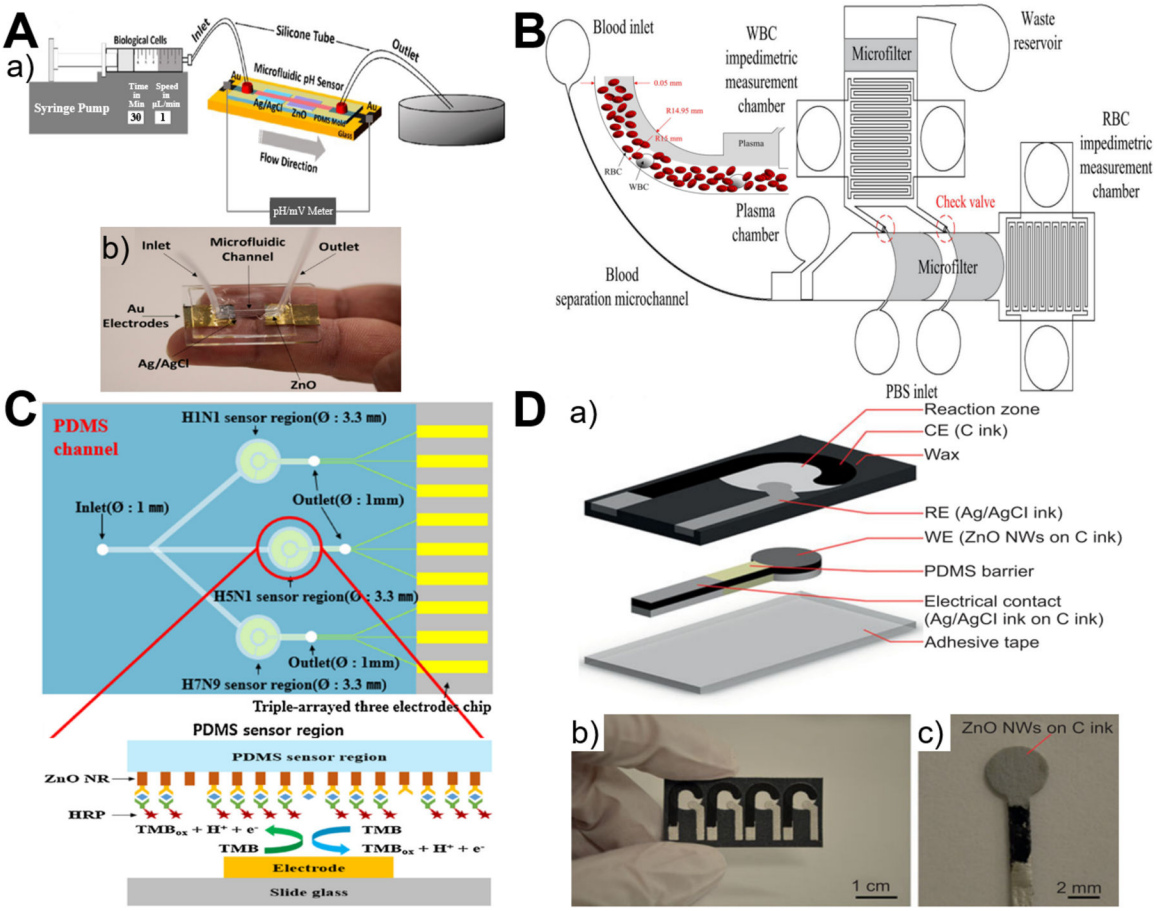

Figure 8.

Microfluidics-enabled electrochemical sensing applications of ZnO materials. (A) Experimental scheme (a) and photograph (b) of ZnO-based microfluidic pH sensor. Reproduced with permissions from reference[94], copyright 2017, American Chemical Society. (B) Measurement of impedimetric ratio of blood cells using microfluidic chip with ZnO nanowires. Reproduced with permissions from reference[98], copyright 2018, Springer Nature. (C) A multi-virus detectable microfluidic electrochemical immunosensor for simultaneous detection of H1N1, H5N1, and H7N9 virus using ZnO nanorods for sensitivity enhancement. Reproduced with permissions from reference[72], copyright 2016, Elsevier. (D) A paper-based microfluidic biosensor integrating zinc oxide nanowires for electrochemical glucose detection. Reproduced with permissions from reference[92], copyright 2015, Springer Nature.

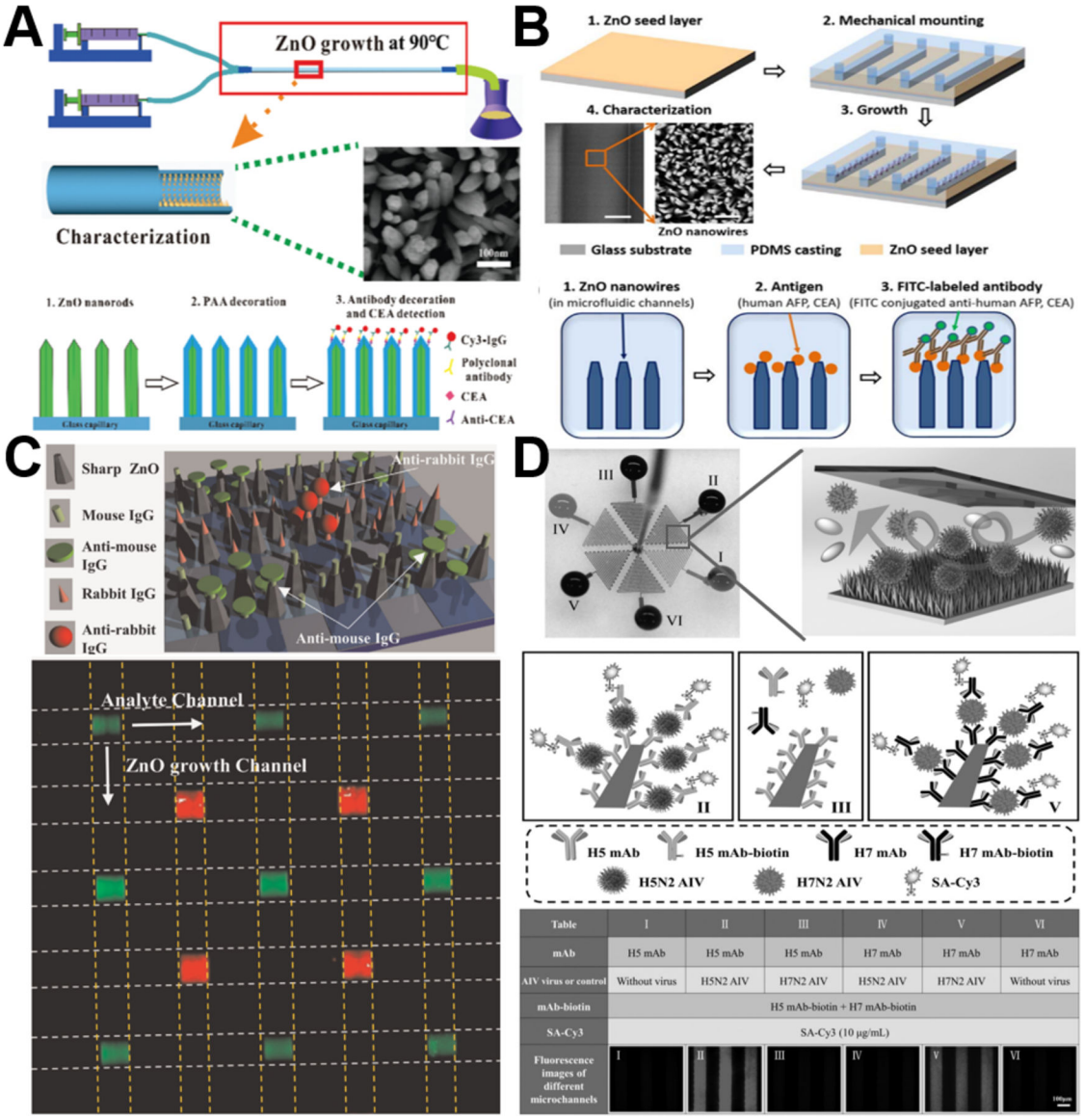

Figure 9.

Microfluidics-enabled immunofluorescent sensing applications of ZnO materials. (A) Enhanced immunofluorescence detection of a protein marker using a PAA modified ZnO nanorod array-based microfluidic device. Reproduced with permissions from reference[80], copyright 2018, Royal Society of Chemistry. (B) Enhanced fluorescence detection of proteins using ZnO nanowires integrated inside microfluidic chips. Reproduced with permissions from reference[78], copyright 2018, Elsevier. (C) Multiple detection of anti-mouse IgG and anti-rabbit IgG using sharp ZnO NWs (a) and fluorescence image of simultaneous multiple protein detection by the microfluidic device (b). Reproduced with permissions from reference[71], copyright 2016, Elsevier. (D) Multiplexed detection of two AIV subtypes of H5N2 and H7N2 in one ZnO nanorods integrated microchip. Reproduced with permissions from reference[96], copyright 2017, John Wiley & Sons.

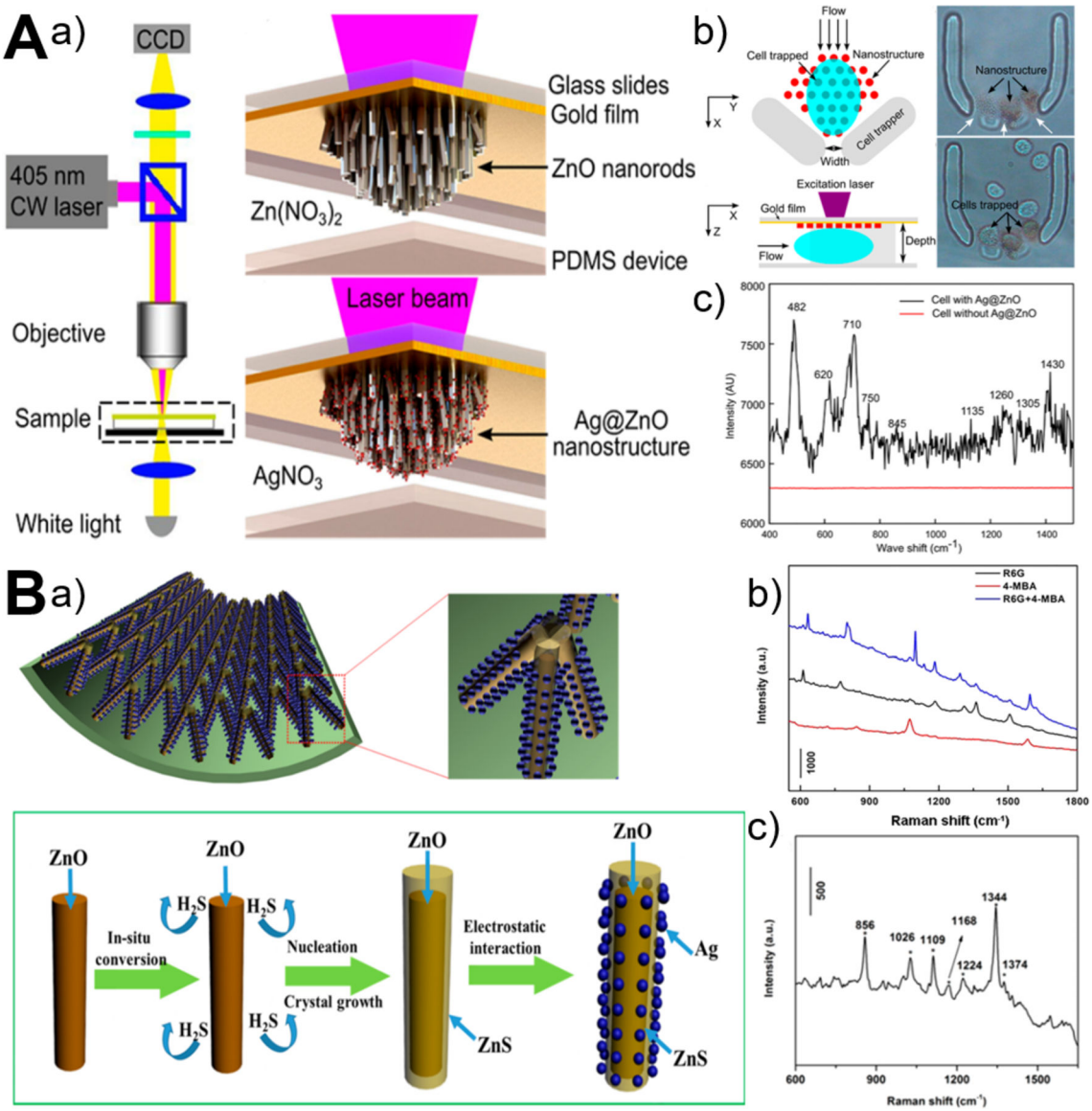

Figure 10.

Microfluidics-enabled SERS sensing applications of ZnO materials. (A) Microfluidic in-situ fabrication of 3D Ag@ZnO nanostructures (a) and SERS fingerprinting of trapped single cells (b,c). Reproduced with permissions from reference[61], copyright 2014, American Chemical Society. (B) Microfluidic capillary synthesis of 3D clustered ZnO@ZnS-Ag nanostructures (a) and SERS sensing performance of R6G, 4-MBA, and MP (b,c). Reproduced with permissions from reference[67], copyright 2016, American Chemical Society.

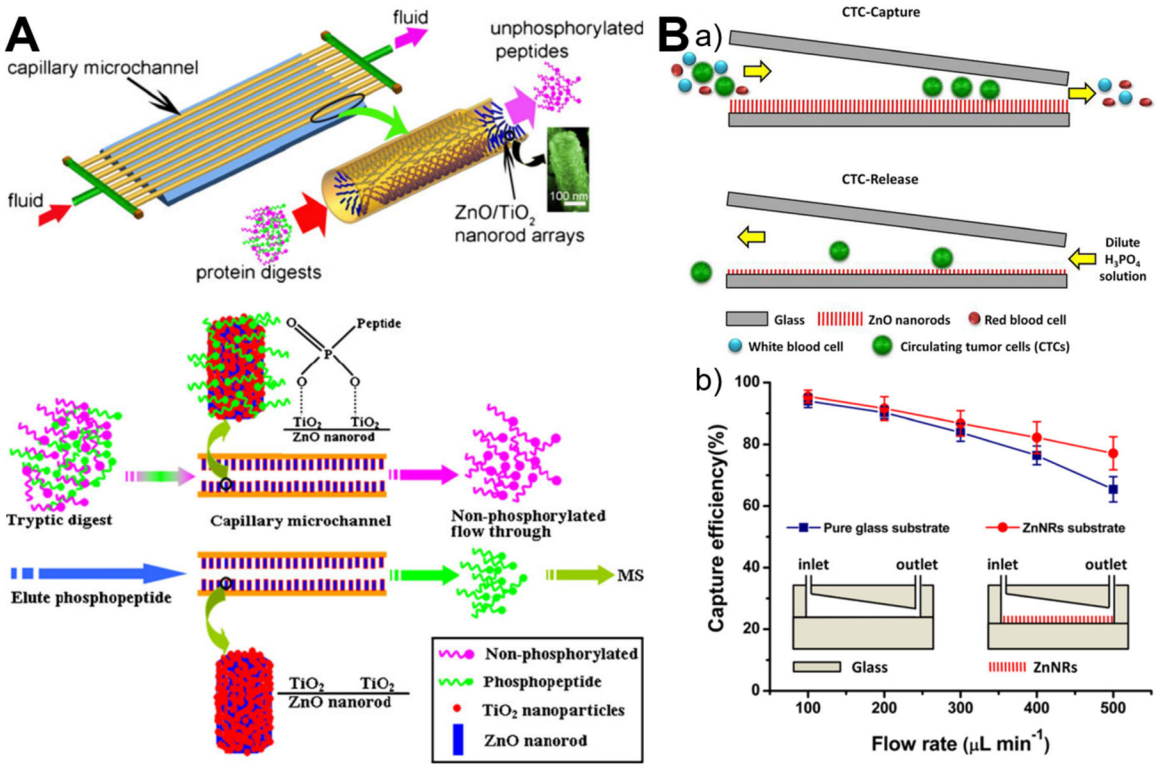

Figure 11.

Microfluidics-enabled biological separation applications of ZnO materials. (A) Continuous high-throughput phosphopeptide enrichment using microfluidic channels modified with aligned ZnO/TiO_2 nanorod arrays. Reproduced with permissions from reference[84], copyright 2011, Springer Nature. (B) Highly efficient isolation and release of circulating tumor cells based on size-dependent filtration and degradable ZnO nanorods substrate in a wedge-shaped microfluidic chip (a), and capture efficiency of spiked SKBR3 cells at different flow rates in two kinds of microfluidic chips with/without ZnO nanorods substrate (b). Reproduced with permissions from reference[95], copyright 2017, Springer Nature.

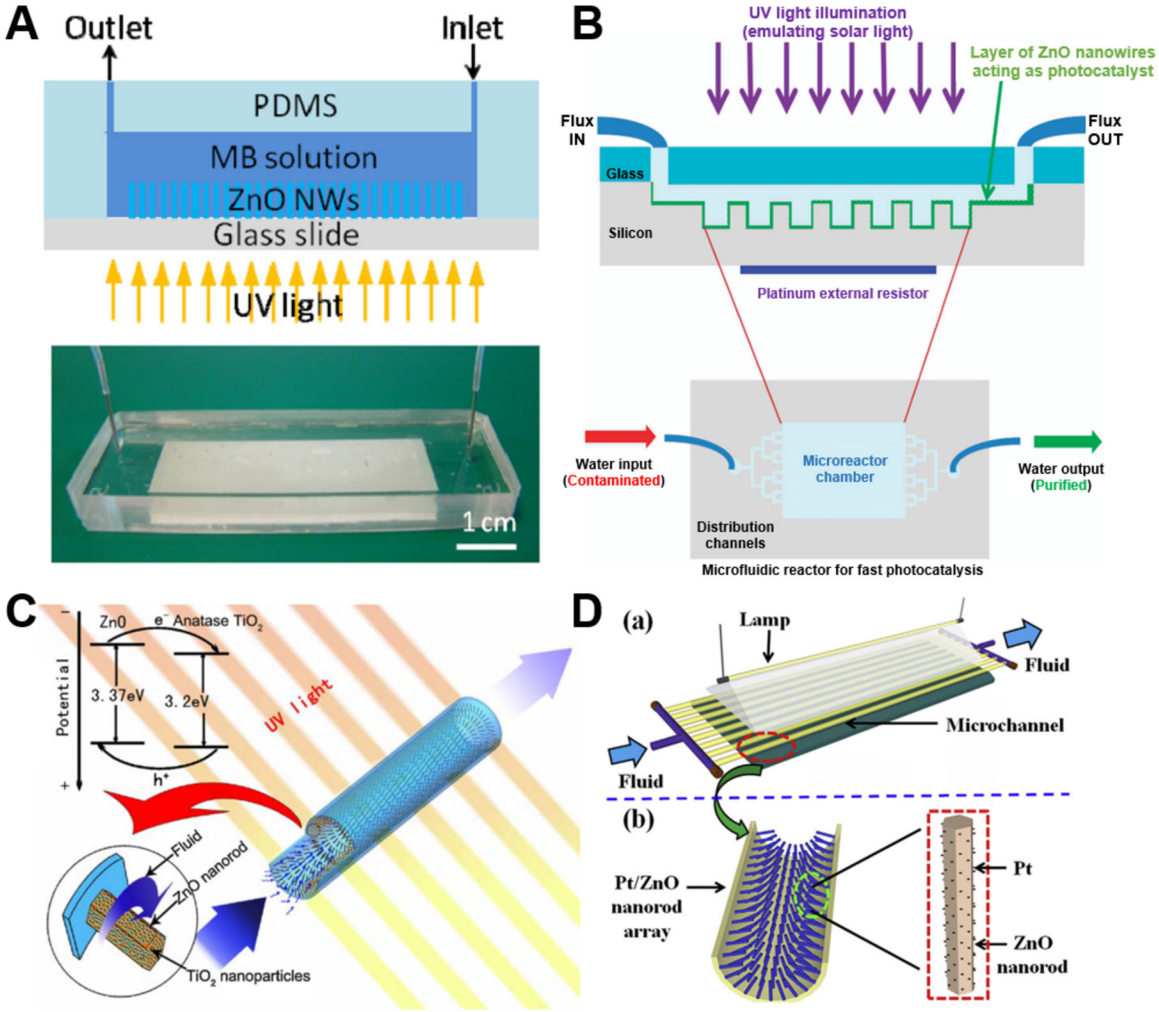

Figure 12.

Microfluidics-enabled catalysis applications of ZnO materials. (A) Microfluidic device with integrated ZnO nanowires for photodegradation of MB. Reproduced with permissions from reference[60], copyright 2013, Elsevier. (B) Schematic illustration of the experimental setup used for water decontamination. The microfluidic reaction chamber including ZnO nanowires acting as photocatalyst is exposed to ultraviolet (UV) light while water is flowing, leading to purified water at the outlet. Reproduced with permissions from reference[79], copyright 2018, Springer Nature. (C) Capillary microchannel-based microreactors with highly durable ZnO/TiO2 nanorod arrays for continuous-flow photocatalysis of MB. Reproduced with permissions from reference[50], copyright 2010, Elsevier. (D) Microreactor with Pt/ZnO nanorod arrays on the inner wall for photodegradation of phenol. Reproduced with permissions from reference[85], copyright 2013, Elsevier.

Table 1:

Synthesis of ZnO materials using microfluidic reactors.

Microreactor type	Particle type	Particle size	Particle shape	Reaction condition	Key precursors	Reference (By year)
T-shaped mixer	ZnO	9 nm	Near-sphere	673 K; 30 MPa	$ZnSO_4$+KOH	2004[46]
T-shaped mixer	ZnO	~3 μm	Flower	90 °C	$Zn(OAc)_2$+NaOH	2008[47]
Microchamber	ZnO	100 nm×(0.5–3 μm)	Wire	90 °C; 0.72–2.88 mL/h	$Zn(NO_3)_2$+HMT	2009[48]
Microchamber	ZnO	(80–100 nm)×(70–860 nm)	Wire	90 °C	$Zn(NO_3)_2$+HMT	2009[49]
Y-shaped mixer	ZnO	(50–100 nm)×1.5 μm	Wire	60–150 °C; 10–25 μL/min	$Zn(OAc)_2$+NaOH; $Zn(NO_3)_2$+HMT	2010[50]
Coflowing reactor	ZnO	~4 nm	Sphere	250 °C; 25 MPa	$Zn(acac)_2$+TOP/OL/OA	2011[51]
T-junction	ZnO	~0.4–4 μm	Sphere; cylinder; star; flower	90–150 °C; 250–3000 μL/min	$Zn(OAc)_2$+NaOH	2011[52]
Straight microchannel	ZnO	(50–100 nm)×(5–6 μm)	Wire	90–95 °C; 0.5–1 μL/min	$Zn(NO_3)_2$+HMT+PEI	2011[53]
Microdot array; Micropost array	ZnO	(100–200 nm)×(2–3 μm)	Wire	95 °C	$Zn(NO_3)_2$+HMT+PEI	2012[54]
T-shaped mixer	ZnO	~5 nm-1 μm	Sphere; tactoid	70 °C; 6.8–28.1 mL/min	$Zn(NO_3)_2$+NaOH	2013[55]
Membrane dispersion reactor	ZnO	7–26 nm	Near-sphere	R.T.; 10–50 mL/min	$ZnSO_4$+NH_4HCO_3	2013[56]
Straight microchannel	ZnO	~80 nm×4 μm	Wire	85–90 °C	DMF	2013[57]
Straight microchannel	ZnO	Up to 11.2 μm in length	Wire	85 °C; 0.55–0.91 mL/min	$Zn(NO_3)_2$+Hexamine	2013[58]
T-shaped mixer	ZnO:Na	3–4 μm	Flower	80 °C; 6.5 mL/min	$Zn(NO_3)_2$+NaOH	2013[59]
Microchamber	ZnO	(100–200 nm)×20 μm	Wire	95 °C	$Zn(NO_3)_2$+HMT+PEI	2013[60]
Microchamber	ZnO	(50–200 nm)×(1–1.5 μm)	Wire	385 K	$Zn(NO_3)_2$+HMT	2014[61]
Y-junction	ZnO	10–20 nm	Near-sphere	40–70 °C; 1–7 mL/min	$Zn(NO_3)_2$/$ZnSO_4$/ $ZnCl_2$+NaOH	2014[62]
T-shaped mixer	ZnO	~3–5 μm	Flower; wire	70 °C; 6.8–28.1 mL/min	$Zn(OAc)_2$+NaOH	2014[63]
T-shaped mixer; winding channel	ZnO	3–5 nm	Sphere	60 °C; 0.855–1.645 μL/min	$Zn(OAc)_2$+NaOH	2014[64]
Straight microchannel	ZnO	50 nm×3 μm	Wire	95 °C; 1–1000 mm/s	$Zn(NO_3)_2$+HMT+PEI	2015[65]
Microchamber	ZnO:Al	(70–140 nm)×(3.9–4.7 μm)	Flake	80 °C; 2 mL/h	$Zn(NO_3)_2$+$Al(NO_3)_3$+NH_4Cl	2015[66]
Y-shaped mixer	ZnO	(100–150 nm)×(1–2 μm)	Wire	60–150 °C; 10–25 μL/min	$Zn(OAc)_2$+NaOH +$Zn(NO_3)_2$+HMT	2016[67]
T-shaped mixer	ZnO	(50–500 nm)×(0.24–16.6 μm)	Wire	70–80 °C; 6.8–28.1 mL/min	$Zn(OAc)_2$+NaOH	2016[68]
T-shaped mixer; cross-type mixer	ZnO-Ag	500 nm	Hedgehog	100 °C; 1 mL/min	$Zn(NO_3)_2$+NaOH +$AgNO_3$+$NaBH_4$	2016[69]

Microreactor type	Particle type	Particle size	Particle shape	Reaction condition	Key precursors	Reference (By year)
Y-shaped mixer	ZnO	2–3 nm	Sphere	180 W ultrasonic power; 20–60 °C	$Zn(OAc)_2$+LiOH	2016[70]
Straight microchannel	ZnO	~100 nm×(1–2 μm)	Sharp end; wire; hexahedral-puncheon	750 μL/h; 60 °C	$ZnSO_4$+NH_4Cl	2016[71]
Microchamber	ZnO	(100–300 nm)×(1–3 μm)	Wire	90 °C	$Zn(NO_3)_2$+HMT	2016[72]
Straight microchannel	ZnO/Zn(OH)F	~40 μm in length	Wire	90 °C; 25 μL/min	$Zn(NO_3)_2$+NH_4F+HMT	2016[73]
Cellulose hydrogel	ZnO	~5 μm	Flower	40–500 °C	$Zn(OAc)_2$+NaOH	2017[74]
Y-shaped mixer	ZnO	10–600 nm	Sphere; sheet; spindle	60 °C; 500 μL/min	$Zn(NO_3)_2$+NaOH	2017[75]
Straight microchannel	ZnO	~1–4 μm in length	Wire	50–60 °C	$ZnSO_4$+NH_4Cl	2017[76]
Flow-focusing with expansion channel	ZnO	145 nm	Rod	100–150 °C	$Zn(acac)_2$+Benzyl alcohol	2018[77]
Straight microchannel	ZnO	160 nm×8.7 μm	Wire	90 °C; 10 μL/min	$Zn(NO_3)_2$+HMT+PEI	2018[78]
Microchamber	ZnO	~1 μm in length	Wire	95 °C	$Zn(NO_3)_2$+HMT	2018[79]
Y-shaped mixer	ZnO-PAA	~100 nm×500 nm	Wire	90 °C; 25 μL/min	$Zn(NO_3)_2$+NH_4OH	2018[80]
Three-channel mixer	ZnO-CuO	~7 nm (crystallite size)	Irregular	70–80 °C; 0.3–0.54 mL/min	$Zn(NO_3)_2$+$Cu(NO_3)_2$+Na_2CO_3	2019[81]
Spiral microchannel	ZnO	~100 nm-2 μm	Sphere; ellipsoid; rod; cube; urchin; platelet	r.t.−80 °C; 2.5–500 μL/min	$Zn(NO_3)_2$+NaOH	2019[82]

Abbreviations: DMF: Dimethyl formamide; HMT: Hexamethylenetetramine; OA: Oleic acid; OL: Oleylamine; PAA: Poly(acrylic acid); PEI: Polyethylenimine; R.T.: Room temperature; TOP: Trioctylphosphine.

Table 2:

Applications of ZnO materials through microfluidic chips.

Microchip type	Material type	Material properties	Application	Target/efficacy	Reference (By year)
Micropump	ZnO	Film (< 6.6 μm thick)	SAW	1 cm/s velocity	2009[83]
Capillary microchannel	ZnO/TiO_2	Nanowire array (1.5 μm thick)	Photocatalysis	100% MB (RT=20 s); >90% (after using for 100 h)	2010[50]
Capillary microchannel	ZnO/TiO_2	Nanowire array (1.5 μm thick)	PP enrichment	50 fmol; 5 cycles	2011[84]
Straight microchannel	ZnO	Nanowire array (5–6 μm thick)	Particle trapping; pH sensing	10 μm particle trapping; pH: 5–9	2011[53]
Straight microchannel	ZnO	Nanowire array (2–3 μm thick)	Cell lysis	Increased protein and nucleic acids concentration	2012[54]
Capillary microchannel	ZnO/Pt	Nanowire array (1–2 μm thick)	Photocatalysis	93% Phenol (RT=180 s); >85% (after using for 110 h)	2013[85]
Microchamber	ZnO	Nanowire array (20 μm thick)	Photocatalysis	96% MB (RT=270 s)	2013[60]
Micropump	ZnO	Film (<6–8 μm thick)	SAW	0.1–90 mm/s velocity	2013[86]
Straight microchannel	ZnO	Nanowire array (4 μm thick)	Photovoltaic cells	Low reflection rates	2013[57]
Microchamber	ZnO-Ag	Nanowire array (1–1.5 μm thick)	Cell trapping; SERS sensing	Hela cell; 4-ATP; BSA (0.01%); DNA (1 μM)	2014[61]
T-type microchannel	ZnO	Nanosphere array (~20 nm)	Electrochemical immunosensing	Thyrotropin (0.00087 μUI/mL)	2014[87]
Straight microchannel	ZnO-PVA	Nanofilm (200 nm thick)	Fluorescent sensing	SYTO 13 dye (1 μM)	2014[88]
Micropump	ZnO	Film (5.5 μm thick)	SAW	1500 m/s velocity	2014[89]
Micropump	ZnO	Film (4 μm thick)	SAW	10 cm/s velocity	2014[90]
Straight microchannel	CuO-ZnO-Al_2O_3/ HZSM-5	Film (20–60 μm thick)	Catalyst	CO conversion; DME production	2015[91]
PAD	ZnO	Nanowire array (~300 nm width)	Electrochemical sensing	Glucose (94.7 μM)	2015[92]
Straight microchannel	ZnO-CuO	Nanowire array (3 μm thick)	Electrochemical sensing	NO_2 (0.1–20 ppm); CO (20–1000 ppm)	2015[65]
Microchamber	ZnO:Al	Nanoflake layer (6 μm thick)	Dye-sensitized solar cells	410% enhancement compared to pure ZnO	2015[66]
Microchamber	ZnO@ZnS-Ag	Nanowire array (1–2 μm thick)	SERS sensing	R6G (10^{-9} M); 4-MBA (10^{-9} M); MP (10^{-8} M); BSA (10^{-8} M)	2016[67]
PAD	ZnO	Nanowire array (4.37 μm thick)	Electrochemical sensing	IgG (60 fg/mL); p24 antigen (300 fg/mL)	2016[93]
Straight microchannel	ZnO	Nanowire array (1–2 μm thick) with sharp end or hexahedral-puncheon	Immunofluorescent sensing	Streptavidin (417 fM); IgG (4.17 pM)	2016[71]
Microchamber	ZnO	Nanowire array (1–3 μm thick)	Electrochemical immunosensing	1 pg/mL H1N1; H5N1; H7N9	2016[72]
Straight microchannel	ZnO/Zn(OH)F	Nanowire array (40 μm thick)	Photocatalysis; protein separation	96% MB (RT=60 s); ~100% hemoglobin (RT=60 s)	2016[73]
Straight microchannel	ZnO	Film (120 nm thick)	pH sensing (CTCs detection)	pH: 1.68–9.18	2017[94]

Microchip type	Material type	Material properties	Application	Target/efficacy	Reference (By year)
Straight microchannel	ZnO	Nanowire array (1–4 μm thick)	Photocatalysis	97% MO (RT=60 s)	2017[76]
Wedge-shaped chip	ZnO	Nanowire array (2 μm thick)	CTCs detection	>87.5% SKBR3; PC3; HepG2; A549	2017[95]
Herringbone chip	ZnO	Nanowire array	Immunofluorescent sensing	H5N2 (3.6×10^3 EID_{50}/mL)	2017[96]
Straight microchannel	ZnO	Nanowire array (~10 μm thick)	Immunofluorescent sensing	AFP (1 pg/mL); CEA (100 fg/mL)	2018[78]
PAD	ZnO-rGO	Nanoflower array (~50 μm thick)	Electrochemical sensing	L-glutamic acid (9.6 pM); L-cysteine (24 pM)	2018[97]
Microchamber	ZnO	Nanowire array (9.14 μm thick)	Electrochemical sensing	Erythrocyte; leukocyte	2018[98]
Microchamber	ZnO	Nanowire array (~1 μm thick)	Photocatalysis	10 ppm Benzene; Toluene; Ethylbenzene; m–p Xylenes; o-Xylene	2018[79]
Straight microchannel	ZnO-PAA	Nanowire array (500 nm thick)	Immunofluorescent sensing	CEA (100 fg/mL)	2018[80]
Fixed-bed reactor	ZnO-CuO	0.1 g catalyst (40–60 mesh)	Catalyst	~1–6 g MeOH per gram catalyst per hour	2019[81]

Abbreviations: AFP: α-fetoprotein; CEA: Carcinoembryonic antigen; CTCs: Circulating tumor cells; DME: Dimethyl ether; MB: Methylene blue; MO: Methyl orange; MP: Methylparathion; PAA: Poly(acrylic acid); PAD: Paper-based analytical device; PP: Phosphopeptide; PVA: Polyvinyl alcohol; rGO: Reduced graphene oxide; RT: Residence time; SAW: Surface acoustic wave; SERS: Surface-enhanced Raman scattering.